

# Symmetry Tests of Rare $\eta$ Decays to All-Neutral Final States

L. Gan (contact person)<sup>1</sup>, A. Gaparian, I. Larin, J. Leckey, D. Mack, R.  
Miskimen, S. Somov, ...

The JLab Eta Factory (JEF) Collaboration

DRAFT April 8, 2012

missing stuff that has to get done before May 4 submission:  
dGamma/dM2g plot with projected errors  
2pi0 continuum plot with more statistics, etc.  
3gamma sims  
updated 3gamma BR sensitivity

---

<sup>1</sup>ganl@uncw.edu

## Executive Summary

Rare decays of the neutral and astonishingly long lived  $\eta$  meson provide a unique, flavor-conserving laboratory to search for new sources of C, P, or CP violation while testing predictions of chiral perturbation theory at high order. Because G parity conservation prevents the  $\eta$  from rapidly decaying to pions by the isospin-conserving strong interaction, the branching ratios for various rare and forbidden  $\eta$  decays are potentially 5 orders of magnitude more sensitive to new interactions than the decays for comparable hadrons. Our three priority physics channels are:  $\eta \rightarrow 2\pi^0$  which is effectively forbidden by known sources of CP violation,  $\eta \rightarrow 3\gamma$  which is effectively forbidden by charge conjugation invariance C, and the rare decay  $\eta \rightarrow \pi^0 2\gamma$  where large contributions begin only at  $O(p^6)$  in chiral perturbation theory. Background studies for these 3 or  $4\gamma$  final states are highly complementary, while the signal from the SM-allowed decay allows us to monitor the quality of the dataset.

No new inventions are required but the technology will be state of the art. Hall D's high energy, tagged photon facility with its planned 30 cm  $LH_2$  target will yield a competitive rate of exclusively produced  $\eta$ 's from forward  $\gamma + p \rightarrow \eta + p$  with good acceptance. However, background reduction compared to older experiments is the main reason the proposed experiment will yield 1-2 orders of magnitude improvement in rare  $\eta$  decays to all-neutral final states. This will be achieved by significantly boosting the  $\eta$ 's and measuring the decay photons in a high granularity, high resolution lead tungstate calorimeter with flash ADC readout on every crystal. The new calorimeter, FCAL-II, will be a larger version of the lead tungstate core of the successful PrimEx HyCal which operated in a similar geometry in Hall B at a similar luminosity (with less sophisticated readout) yet encountered only 0.5% pile-up.

Boosted  $\eta$ 's not only provide insensitivity to detector thresholds and low energy backgrounds, but cause  $\eta \rightarrow 3\pi^0$  decays with missing photons to fall safely out of the  $\eta$  invariant mass cut. The invariant mass resolution with lead tungstate is over a factor of 2 better than lead glass. The small crystal size and 6m target-to-calorimeter distance greatly reduce a potentially important background from  $\eta \rightarrow 3\pi^0$  with shower merging. Good resolution plus measurement of the recoil proton for larger  $\eta$  angles will control the background from continuum  $\gamma + p \rightarrow 2\pi^0 + p$ . Although the allowed decay  $\eta \rightarrow 4\gamma$  is a potential background, it has never been seen and calculations suggest it is highly suppressed.

# 1 Physics Motivation and Overview

The goal of our proposal is to make revolutionary improvements in  $\eta$  rare decay measurements to all-neutral final states to improve our knowledge of QCD and tighten the presently modest model-independent constraints on new sources of C, P, and CP violation in hadron decays. Specifically, we will measure the allowed  $\eta \rightarrow \pi^0\gamma\gamma$  decay width and its differential decay width  $d\Gamma/dM_{2\gamma}$  with sufficient precision to tightly constrain chiral perturbation theory calculations of this highly suppressed process. In doing so, we will improve the upper limits on the Standard Model (SM) forbidden channels  $\eta \rightarrow \pi^0\pi^0$ ,  $\eta \rightarrow \pi^0\gamma$  and  $\eta \rightarrow 3\gamma$  by up to 2 orders of magnitude. These seemingly disparate physics goals are quite complementary: the background studies overlap, a sensitive measurement in one channel implies high sensitivity in the others, and the allowed  $\eta \rightarrow \pi^0\gamma\gamma$  decay allows us to not only monitor data quality but reduce uncertainties in the SM background calculations for other new physics searches such as  $K^0 \rightarrow \pi^0 l^+ l^-$ . Although rare decays of the  $\eta$  are an active field of research at other laboratories, the sensitivity of the all-neutral program outlined here cannot be matched without Hall D's high energy, high intensity, tagged photon beam combined with the proposed high resolution, high granularity calorimeter with flash ADC readout on every crystal.

## 1.1 The $\eta$ meson and Standard Model Tests

While the SM has been successful in explaining many phenomena to high accuracy, it offers no insight into experimental facts such as the dominance of matter over anti-matter, the nature of dark matter needed to explain the rotation curves of the galaxies, nor dark energy which causes the accelerated expansion of the universe. Searching for physics beyond the SM is thus a well-motivated and important task for physicists. A sensitive means of searching for new physics is through tests of fundamental symmetries such as chiral symmetry, charge conjugation C, parity P, and time reversal T, as well as CP and CPT. Enormous investments have been made in flavor-changing decays in K and B mesons, as well as weak decays of the lightest mesons, the pion and muon, with no uncontroversial evidence found for new physics. Those programs are well-motivated and must continue since sufficiently precise and/or sensitive measurements at the weak scale ( $\sim 100$  GeV) constrain the possibility of new semi-leptonic and leptonic interactions at the TeV-scale. (Indeed, measurements of helicity suppressed rare decays can constrain new interactions at the 10-100 TeV scale.) However, the sector of flavor-conserving, non-weak decays has not been as thoroughly exploited. This presents an opportunity for JLab's Hall D.

One distinguishing feature of the  $\eta$  meson which makes it a unique probe for new physics is directly related to its birth. In the chiral limit, the condensation of quark-antiquark pairs in the QCD vacuum spontaneously breaks  $SU_L(3) \times SU_R(3)$  symmetry down to the flavor

Mode	Branching Ratio	Symmetry Highlight	Role in Proposal
$\pi^0 2\gamma$	$(2.7 \pm 0.5) \times 10^{-4}$	$\chi$ PTh, $\mathcal{O}(p^6)$	priority
$\pi^0 \pi^0$	$< 3.5 \times 10^{-4}$	CP, P	priority
$4\pi^0$	$< 6.9 \times 10^{-7}$	CP, P	ancillary
$\pi^+ \pi^-$	$< 1.3 \times 10^{-5}$	CP, P	— (lowest upper limit for $\pi\pi$ )
$4\gamma$	$< 2.8 \times 10^{-4}$	suppressed ( $< 10^{-11}$ )	ancillary
$\pi^0 \gamma$	$< 9 \times 10^{-5}$	C, L	priority (control)
$3\gamma$	$< 1.6 \times 10^{-5}$	C	priority
$2\pi^0 \gamma$	$< 5 \times 10^{-4}$	C	ancillary
$3\pi^0 \gamma$	$< 6 \times 10^{-5}$	C	ancillary
$\pi^0 e^+ e^-$	$< 4 \times 10^{-5}$	C	—
$e^+ e^-$	$< 2.7 \times 10^{-5}$	helicity suppressed	—

Table 1: Some  $\eta$  rare decays to all-neutral final states, their role in this proposal, plus a few closely related channels [8]. The PDG branching ratio for  $\pi^0 2\gamma$  is the average of several widely inconsistent measurements as suggested below in Figure 2. The theoretical upper limit for the  $\eta \rightarrow 4\gamma$  decay is estimated from a  $\pi^0$  calculation[23]. Final states with  $e^+e^-$  pairs have closely related physics goals but require background simulations which are beyond the scope of this proposal.

$SU(3)$  symmetry. As a result, there are eight massless Goldstone Bosons corresponding to the eight spontaneously broken symmetry generators. These Goldstone Bosons are identified with the octet of pseudoscalar mesons ( $\pi^0$ ,  $\pi^\pm$ ,  $K^\pm$ ,  $K^0$ ,  $\bar{K}^0$ , and  $\eta$ ). In reality, the quark masses are non-zero (albeit small), thus breaking the chiral symmetry explicitly and giving rise to masses for the Goldstone Bosons following the mechanism discovered by Gell-Mann, Oakes and Renner [1]. As the most massive member in the octet pseudoscalar meson family, the  $\eta$  is more sensitive to QCD symmetry breaking.

Another distinguishing feature of the  $\eta$  is that all its strong and electromagnetic decays are forbidden in lowest order due to P, C, CP, G-parity and angular momentum conservation [2]. This obviously enhances the relative importance of higher order processes. The width of the  $\eta$  ( $\Gamma_\eta = 1.3$  KeV) is about five orders of magnitude smaller than the  $\rho$  meson ( $\Gamma_\rho = 149$  MeV), for example. All other things being equal, this makes measurements of branching ratios or upper limits of various rare and forbidden  $\eta$  decays about 5 orders of magnitude more sensitive to new interactions. The potential of a broad program of  $\eta$  rare decay studies has been discussed by Kullander *et al.*[3] and Nefkens and Price[2]. The status has evolved since those articles were written due to results from KLOE and BES plus new initiatives in Europe such as the Crystal Ball at MAMI[4] and WASA at COSY[5].

Table 1.1 shows various  $\eta$  rare decays of relevance to this proposal. Our flagship channels will be the all-neutral final states (with 3 or 4  $\gamma$ 's)  $\eta \rightarrow \pi^0\gamma\gamma$ ,  $\pi^0\pi^0$ , and  $3\gamma$  to investigate chiral symmetry breaking, P and CP, and C violation respectively. We anticipate that significant improvements in several ancillary channels will result as well, particularly those which had large backgrounds in previous experiments such as  $\eta \rightarrow 4\gamma$  and  $\eta \rightarrow 2\pi^0\gamma$ . Each will require its own careful yet complementary analysis of backgrounds. This program will provide a great opportunity to better understand the symmetry structure of QCD while expanding the search for new physics in flavor-conserving, non-weak decays.

Based on the C and P conservation selection rules given in the Appendix, all neutral final states with up to 4  $\pi^0$ 's and/or up to 4  $\gamma$ 's are listed in Table 7. All branching ratio upper limits in this proposal are quoted at 90% confidence level.

## 1.2 The rare decay $\eta \rightarrow \pi^0\gamma\gamma$

The decay  $\eta \rightarrow \pi^0\gamma\gamma$  is sufficiently suppressed that, while it has been relatively straightforward to observe a non-zero signal, measurements accurate enough to challenge chiral perturbation theory have proven elusive. In addition to its own significant scientific merit, this channel serves as a stepping stone to optimize the experimental design for other decay channels effectively forbidden in the SM with a similar number of final state  $\gamma$ 's.

This “doubly radiative”  $\eta$  decay has a dramatic history spanning more than four decades [9] and has attracted much attention from both theorists and experimentalists. In chiral perturbation theory (ChPT), the tree level amplitudes vanish at both  $\mathcal{O}(p^2)$  and  $\mathcal{O}(p^4)$ , and the first non-vanishing contribution comes from  $\mathcal{O}(p^4)$  loop terms [10]. However, loops involving kaons are largely suppressed due to the large kaon mass, while the pion loops are suppressed due to G parity. The first sizable contribution comes at  $\mathcal{O}(p^6)$ , hence this channel provides a unique probe for higher order corrections in ChPT. Because  $\mathcal{O}(p^6)$  coefficients are not all known, these effects cannot be calculated model independently. A recent article by Oset *et al.* demonstrates how the shape of the two-photon invariant mass spectrum,  $d\Gamma/dM_{2\gamma}$ , probes the underlying dynamics [11]. (See Fig 1.) Because this spectrum provides much more information than the simple branching ratio, precise measurements would be very desirable.

### 1.2.1 status of $\eta \rightarrow \pi^0\gamma\gamma$ measurements

About two dozen experiments have been performed to measure this decay width since 1966. After considerable effort, the first significantly sensitive result was published by the GAMS-2000 collaboration [12] in 1984 yielding  $\Gamma(\eta \rightarrow \pi^0\gamma\gamma) = 0.84 \pm 0.18$  eV, about two times larger than the average of the ChPT predictions as shown in Figure 2. By contrast, the average of more recent results from the Crystal Ball and KLOE collaborations is about

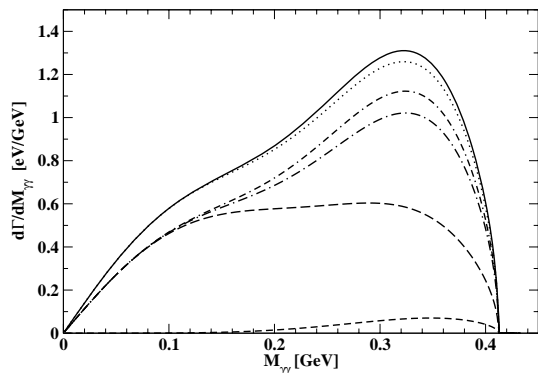


Figure 1: Predicted two-photon invariant mass distribution [11]. From bottom to top, the short-dashed line is for chiral loops, the long-dashed line is tree-level VMD, the dashed-dotted line is the coherent sum of the previous two, the double dashed-dotted line is the same but with VMD loops added, the solid line is the same but with the anomalous terms added. The dotted line is the same as the solid line but substituting the  $K^+K^- \rightarrow \eta\pi^0$  amplitude by its lowest order.

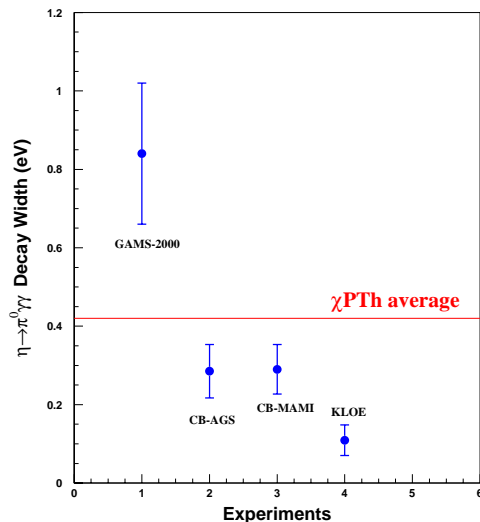


Figure 2: Experimental results on the decay width of  $\eta \rightarrow \pi^0\gamma\gamma$ . From left to right, the points are from GAMS-2000 [12], the Crystal Ball collaboration at the AGS [13][14], the Crystal Ball collaboration at MAMI [15], and KLOE [16]. The red solid line is the average result of ChPT predictions.

half the theoretical prediction. Even these more recent results are inconsistent between the Crystal Ball and KLOE collaborations, with central values differing by a factor of 3 at high confidence.

The discrepancies are almost certainly due to large backgrounds in the older experiments, including a class of backgrounds which can peak beneath the signal. (See our simulations in Figure 7 of Section 2.) A new experiment with a revolutionary reduction in backgrounds would provide greatly reduced statistical and systematic errors leading to a definitive result for the  $\pi^0 2\gamma$  decay width. At the same time, this improved capability is expected to allow us to reduce the upper limits for several all-neutral CP and C forbidden decays by up to 2 orders of magnitude.

### 1.3 The CP violating decay $\eta \rightarrow \pi^0\pi^0$

Another interesting four-photon final state reaction is  $\eta \rightarrow \pi^0\pi^0$  which would violate P

while conserving C and thus violate CP. (See Appendix A.1 for discussion of selection rules in  $\eta \rightarrow N\pi^0$ .) Since the discovery of a 0.2% CP violation in 1964 came as a great surprise, the origin of this violation remains one of the most mysterious phenomena in elementary particle physics. In the Standard Model, CP symmetry is broken by a single complex phase in the Yukawa couplings. In the basis of mass eigenstates, this single phase appears in the Cabibbo-Kobayashi-Maskawa quark matrix (CKM) that gives the W-boson couplings to an up-type antiquark and a down-type quark, known as the Kobayashi-Maskawa (KM) mechanism. This violation shows up in flavor-changing interactions. For flavor-conserving processes, CP violation is minute because it requires a two-step change of flavor – a first step to an intermediate flavor state and a second to return to the initial flavor state [18]. As a result, SM sources for a CP violating decay like  $\eta \rightarrow \pi^0\pi^0$  are expected to lead to an unobservably small branching ratio, at the level of  $2 \times 10^{-27}$  [18].

CP violation was originally observed in neutral  $K$  decays, and more recently in  $B$  decays. These results provide a model-independent proof that the KM mechanism is the dominant source of CP violation in flavor changing decays. Despite the phenomenological success of the KM mechanism, however, it fails by several orders of magnitude to explain the matter-antimatter asymmetry of the Universe. Most extensions of the Standard Model imply additional sources of CP violation. The search for new sources has motivated intensive investigations in flavor-changing sector, such as  $K$ ,  $B$ , and  $D$  meson decays, and no new source of CP violation has yet been discovered. Since the KM source of CP violation dominates in flavor-changing processes, state-of-the-art rare kaon decay measurements are made in the context of a large SM “background” which must be calculable for the results to be interpretable. The SM ambiguities from long distance effects in relatively low background reactions like  $K_L^0 \rightarrow \pi^0 l^+ l^-$  have shifted priorities to the more interpretable but even more difficult to measure  $K_L^0 \rightarrow \pi^0 \nu \bar{\nu}$ .<sup>2</sup> Nevertheless, the  $K_L^0 \rightarrow \pi^0 l^+ l^-$  channels provide sensitivity to different short distance operators so provide complementary information to  $K_L^0 \rightarrow \pi^0 \nu \bar{\nu}$  [6],[7].

The decay of  $\eta \rightarrow 2\pi^0$  is among the few possible flavor-conserving tests listed in the Review of Particle Physics to search for non-conventional CP violation [20]. The long lifetime of the  $\eta$  makes it the must-do candidate. However, because  $\eta \rightarrow 2\pi^0$  is flavor conserving and proportional to the *square* of  $\theta_{QCD}$ , constraints on  $\theta_{QCD}$  from neutron EDM experiments are extremely tight. A SM extension including spontaneous CP violation in the Higgs sector and a  $\theta_{QCD}$  term [19][21] predicts  $BR(\eta \rightarrow \pi^0\pi^0) \sim 10^{-15}$ , about  $10^{12}$  times larger than the KM alone yet still far below the sensitivity of any conceivable  $\eta \rightarrow 2\pi^0$  search.

To evade constraints on light quark CP violation from neutron EDM measurements, a natural approach is to invoke the  $s\bar{s}$  content of the  $\eta$  which is responsible for most of

---

<sup>2</sup>In the virtual decay  $K_L^0 \rightarrow \pi^0 2\gamma$  the  $2\gamma$  can decay or rescatter to  $l^+ l^-$  but not  $\nu \bar{\nu}$  since the SM neutrino has no charge or magnetic moment.

its mass. For the allowed decay  $\eta \rightarrow \pi^+\pi^-\gamma_{R,V}$  (BR = 4.6%), two papers have calculated photon decay asymmetries assuming a flavor-conserving, CP-violating, four quark operator proportional to a new coupling constant  $G$ . [22] (At the cartoon level, a strange quark loop annihilates into light  $q\bar{q}$  pairs to form pions.) Since  $G$  was virtually unconstrained by existing data and taken to be  $O(1)$ , the allowed asymmetries were proportional to  $G^1$  and sizeable. Unfortunately, no such calculation has been done for  $\eta \rightarrow 2\pi^0$  although one assumes the result will be proportional to  $G^2$ .

A calculation is needed to understand our sensitivity in the context of the  $s\bar{s}q\bar{q}$  operator mentioned in the previous paragraph. However, our motivation is model independent: as long as the source of the matter-antimatter asymmetry in the universe is unresolved, the few tests of CP which nature has allowed us, both flavor violating and flavor conserving, must be fully exploited.

To conclude this section, the decay channels  $\eta \rightarrow 2, 4\pi^0$  are unique, flavor-conserving ways to search for new sources of CP violation, and there is a plausible mechanism for avoiding the constraints from neutron EDM.

### 1.3.1 status of CP violation searches

To be filled out later:

The current experimental limit on  $\eta \rightarrow 2\pi^0$  is  $3.5 \times 10^{-4}$  [8].

The limit on the charged channel  $\eta \rightarrow \pi^+\pi^-$  is much lower,  $1.3 \times 10^{-5}$ .

EDITOR'S NOTE: COMPARATIVE FIGURE OF MERIT PLOT GOES HERE (MACK)

## 1.4 The C non-invariant decays $\eta \rightarrow \pi^0\gamma$ and $\eta \rightarrow 3\gamma$

The charge conjugation operation, C, effectively replaces all particles by their antiparticles in the same state. Relatively few systems are suitable for tests of the non-invariance of C because one requires a particle of good C (or self-conjugate composite system) whose decay into a state of well-defined but opposite C is blocked *only* by C invariance. [25] Experimental precision is limited by the need to first produce these unusual systems then search for the relevant decay branches with high efficiency while keeping backgrounds low. A classic example of a purely leptonic self-conjugate system is  $e^+e^-(ortho) \rightarrow 2\gamma$ . Comparisons of Hydrogen and anti-Hydrogen properties have more recently allowed tests of C in atomic systems. The present proposal intends to improve limits for non-weak decays of hadrons using  $\eta \rightarrow 3\gamma$ .

Within the SM, C conjugation is maximally violated in the weak interaction (usually

accompanied by P violation so that CP is conserved). Both C and P are generally assumed to be exact symmetries in the strong and electromagnetic interactions despite the fact that the experimental bounds have not reached the level of 0.1% by amplitude. In addition to  $\eta \rightarrow 3\gamma$ , we will search for another 3 photon final state forbidden by charge-conjugation invariance,  $\eta \rightarrow \pi^0\gamma$ . (See Appendix A.2,3 for discussion of selection rules in  $\eta \rightarrow 3\gamma$  and  $\eta \rightarrow \pi^0\gamma$ .) However, since the latter is also forbidden by the conservation of angular momentum (respected by most but not all SM extensions), we assume it will serve as an experimental control.

Before one can search for new sources of C violation, one must have an estimate for the SM background. The only known source of C violation is the weak interaction. Dicus [26] estimated the ratio  $\Gamma(\pi^0 \rightarrow 3\gamma)/\Gamma(\pi^0 \rightarrow 2\gamma) = 10^{-31}$  by applying dimensional arguments to the SM parity violating interaction including Bose symmetry. A similar estimate can be done for the  $\eta \rightarrow 3\gamma$  process by substituting the  $\eta$  mass for the  $\pi^0$  mass yielding  $\Gamma(\eta \rightarrow 3\gamma)/\Gamma(\eta \rightarrow 2\gamma) = 10^{-24}$ . Despite the enormous enhancement in this branching ratio for the  $\eta$ , and considerable uncertainty in the original estimate<sup>3</sup>, the SM background for  $\eta \rightarrow 3\gamma$  is effectively zero. Thus any non-zero result for  $\eta \rightarrow 3\gamma$  would require a new source of C violation.

#### 1.4.1 previous tests of C non-invariance and their Figures of Merit

The lowest upper limit in any pseudo-scalar meson decay,  $3.1 \cdot 10^{-8}$ , was obtained over two decades ago in  $\pi^0 \rightarrow 3\gamma$  using the Crystal Box at LAMPF[27]. Neutral pions were produced by the reaction  $\pi_{stopped}^- + p \rightarrow \pi^0 + n$ . Accounting for the fact that the acceptance due to geometry plus cuts was only 0.01, there were effectively  $1.2 \cdot 10^8$   $\pi^0$ 's produced. The background was extremely low with only 4 counts in the signal window. This was in part due to the limited number of open channels for  $\pi^0$  decay, but also due to good design and stringent cuts. The photon detector consisted of NaI(Tl) with one TDC and two ADCs per channel; the comparison of an on-time gate with a delayed gate helped flag pile-up. The 250 MHz Flash ADCs we will use in Hall D on every crystal will provide comparable energy and timing information but with much greater discrimination against pile-up.

Due to the larger number of open channels in  $\eta$  decay, it would be a great challenge to match the precision of the  $\pi^0 \rightarrow 3\gamma$  experiment in  $\eta \rightarrow 3\gamma$ . Without a specific mechanism for a new source of C violation however, the  $\eta \rightarrow 3\gamma$  reaction may be able to evade constraints from the superb LAMPF  $\pi^0 \rightarrow 3\gamma$  measurement. Some evasion could be simply be kinematic: we saw from the earlier SM estimate for the BR( $\pi^0 \rightarrow 3\gamma$ ) by Dicus how a rare process could contain many powers of the meson mass giving radically different branching ratios for the  $\pi^0$  and  $\eta$ . Evading constraints could also take dynamical form if for example the greater  $s\bar{s}$

---

<sup>3</sup>The uncertainty was  $\pm 6$  orders of magnitude due in part to the somewhat arbitrary choice of effective quark mass in the loop

content of the  $\eta$  turned out to be a new C violation source.

In the  $\eta \rightarrow 3\gamma$  regime, the most precise upper limit of  $1.6 \cdot 10^{-5}$  was set by the KLOE detector at the Frascati  $\phi$ -factory *DAΦNE*[28]. That experiment produced  $1.8 \cdot 10^7$   $\eta$ 's in 2001-2 by the  $e^+ + e^- \rightarrow \phi \rightarrow \gamma + \eta$  process (BR 1.3%). Photons were detected in a lead/scintillating fiber sampling calorimeter. With an estimated acceptance of 20% for  $\eta \rightarrow 3\gamma$ , there were effectively  $3.6 \cdot 10^6$   $\eta$ 's produced, similar to the effective  $\eta$  production from half a year of JEF operation. The unique KLOE background in the  $3\gamma$  final state was dominated by  $e^+ + e^- \rightarrow \omega\gamma \rightarrow \pi^0\gamma + \gamma \rightarrow 4\gamma$  where one of the  $\gamma$ 's tagged an  $\eta$  that did not exist. The signal window contained no significant excess above a background of 1513 counts (0.042% of the accepted  $\eta$ 's).

The Crystal Ball experiment at BNL AGS set a somewhat weaker upper limit on the existence of the  $\eta \rightarrow 3\gamma$  process of  $4 \cdot 10^{-5}$ [29]. Photons were detected in an array of NaI(Tl) crystals. There was an ADC for each crystal, but only one TDC per group of 9 crystals. That experiment produced  $2.8 \cdot 10^7$   $\eta$ 's via the  $\pi^- + p \rightarrow \eta + n$  reaction at threshold. With an estimated acceptance of 10% for  $\eta \rightarrow 3\gamma$ , there were effectively  $2.9 \cdot 10^6$   $\eta$ 's produced (similar to KLOE). The dominant background was from  $\pi^- + p \rightarrow 2\pi^0 + n$  continuum production, followed by the merging or loss of a low energy photon. Other, much smaller, backgrounds in the Crystal Ball experiment arose from the merging of showers from the large branch  $\eta \rightarrow 3\pi^0 \rightarrow 6\gamma$  or splitting of a photon from the large branch  $\eta \rightarrow 2\gamma$ . A unique background in this experiment was  $\pi^- + p \rightarrow \pi^0 + n \rightarrow 2\gamma + n$  where the  $n$  was detected in coincidence with the photons. It was easily suppressed to a negligible level by cuts.

The backgrounds of relevance to JEF will be qualitatively similar to the non-unique backgrounds at the Crystal Ball. These backgrounds should be greatly reduced at JLab due to our high granularity calorimeter which reduces photon merging, our “boosted  $\eta$ ” kinematics which immensely reduces the phase space for a photon to fall out of the acceptance and remain within our missing energy or invariant mass cuts. We also have the option of detecting the recoil proton at larger  $\eta$  angles to ensure it is consistent with the 2-body reaction  $\gamma + p \rightarrow \eta + p$  rather than 3-body  $\gamma + p \rightarrow 2\pi^0 + p$ . Having a flash ADC per channel will also allow us to flag pile-up in the offline analysis.

EDITOR’S NOTE: COMPARATIVE FIGURE OF MERIT PLOT GOES HERE (MACK)

## 2 Controlling Backgrounds: The $\pi^0 2\gamma$ Case

As in any rare decay experiment, the major challenge is to suppress backgrounds while maintaining high efficiency for the reaction of interest. All our priority  $\eta$  decay channels require photon detection. In the following sections, we employ the allowed channel  $\eta \rightarrow \pi^0\gamma\gamma$

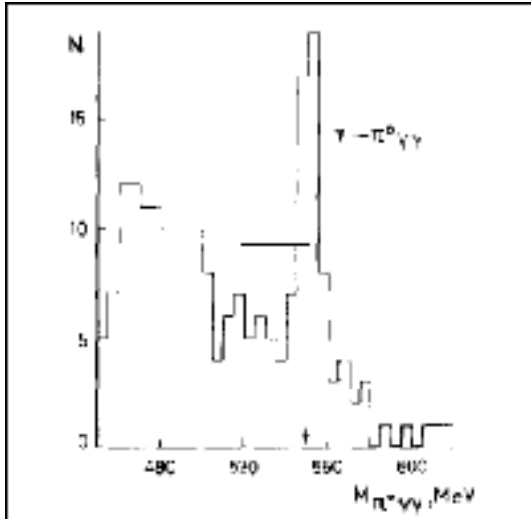


Figure 3: Invariant mass spectrum for the  $\pi^0\gamma\gamma$  reaction measured by the GAMS collaboration [12] using high energy  $\eta$  production via  $\pi^- + p \rightarrow \eta + n$ .

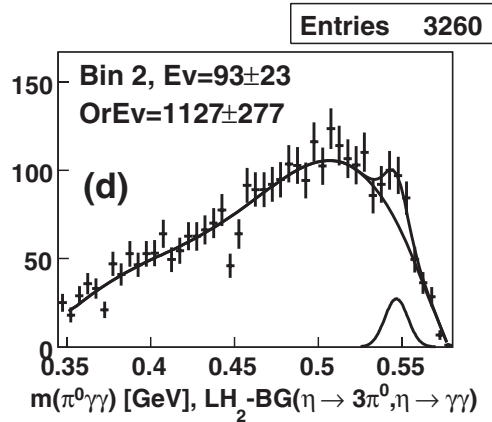


Figure 4: Invariant mass spectrum for the  $\pi^0\gamma\gamma$  system measured by the Crystal Ball collaboration at the BNL AGS [14] with  $\eta$ 's produced near threshold via  $\pi^- + p \rightarrow \eta + n$ .

to highlight the unique experimental challenges of such experiments and explain how our proposal addresses them.

Previous  $\eta \rightarrow \pi^0\gamma\gamma$  experiments [12][14][16] found the largest background to be from  $\eta \rightarrow 3\pi^0$  which has a branching ratio about three orders of magnitude larger than the desired  $\eta \rightarrow \pi^0\gamma\gamma$  decay. Obviously, for a  $6\gamma$  decay to be a background to a  $4\gamma$  process, two photons must effectively go uncounted while (somewhat paradoxically) the reconstructed invariant mass remains close to the  $\eta$  mass. There are two different mechanisms for this [12]: 1) a soft photon falls out of the geometrical acceptance or below threshold of the detector, or 2) two photons merge into what appears to be a single shower.

The first mechanism (the loss of photons) is a major problem in experiments that produce the  $\eta$ 's with small or modest boost (which describes the majority of published work). In that case, decays frequently produce low energy  $\gamma$ 's whose omission allows the the  $\eta \rightarrow 3\pi^0$  background to pass missing energy or  $\eta$  invariant mass cuts. The second mechanism, the merging of photons, is a problem when individual crystals subtend too large a solid angle, a feature of the legacy Crystal Ball calorimeter which was not originally designed for  $\eta$  decay experiments. Both mechanisms can be greatly suppressed by increasing the energy of the  $\eta$  mesons while maintaining sufficient granularity in the calorimeter.

The advantage of using highly boosted  $\eta$ 's can be seen by comparing the results from two older experiments shown in Figure 3 and Figure 4. The figure from GAMS (on the left) shows

a narrow peak from  $\eta \rightarrow \pi^0 \gamma \gamma$  which is 7x larger than a smoothly falling background. [12] In that experiment, the  $\eta$ 's were produced by a high energy  $\pi^-$  beam (30 GeV/c) in the charge exchange reaction  $\pi^- p \rightarrow \eta n$ . The decay photons from  $\eta$  decays were detected in the forward direction by a calorimeter consisting of a 48 module x 32 module matrix of lead glass. Because of the boost, when a photon is lost the effect on the  $\eta$  mass reconstruction is relatively large thus the background from missing photons in  $\eta \rightarrow 3\pi^0$  events is shifted well below the  $\eta$  mass.

In the Crystal Ball [14] and KLOE[16] experiments at the AGS and DAΦNE, respectively, the  $\eta$ 's were produced with very little boost so the energy of the decay  $\gamma$ 's was  $\sim 50$ – $500$  MeV. Under these circumstances, the background from  $\eta \rightarrow 3\pi^0$  is broadly peaked near the  $\eta$  mass peak as can be seen in Figure 4.<sup>4</sup> The background is not only relatively large; our simulations show that when photons merge there is a peaking component which is indistinguishable from the signal. In that case case, sideband subtractions alone are unreliable and one must rely on simulations of shower merging probability. Under such background conditions it is already difficult to accurately determine the simple branching ratio. The measurement of accurate  $d\Gamma/dM_{\gamma\gamma}$  spectra to probe the dynamics of the decay is even more difficult.

As described above, the second important mechanism for  $\eta \rightarrow 3\pi^0$  to mimic the  $\eta \rightarrow \pi^0 \gamma \gamma$  decay is through overlapping photon clusters in the  $\gamma$  detector. The most practical size for a calorimeter element is set by the Moliere radius which, loosely speaking, describes the radial extent of the shower core.<sup>5</sup>  $PbWO_4$  crystals have Moliere radii ( $\sim 2$  cm) about two times smaller than the typical material (such as lead glass) used in an older generation calorimeters. The alert reader will note that this benefit is apparently offset by kinematic focusing from our highly boosted  $\eta$ 's. However, we win because we have moved the calorimeter far from the target center (6m), hence the decay products are distributed over 3445 crystals each with transverse dimensions of roughly a Moliere radius. By contrast, the Crystal Ball detector with acceptance of 93% of  $4\pi$ , has only 672 NaI(Tl) crystals. Another advantage we have is algorithms developed by PrimEx to use measured radial energy profiles to identify pairs of showers separated by only a few cm. To conclude, the JEF configuration tightly manages the potentially serious problem of photon merging in rare  $\eta$  decays. As we will see below, this leaves a small peaking background in the invariant mass spectrum which we will be able to accurately simulate and subtract.

Before discussing our Monte Carlo simulations, we need to introduce the elasticity parameter which is the basis for an important cut. In our forward, high energy kinematics, the  $\eta$  carries almost the full beam energy. This means that the elasticity, defined as  $\Sigma E_\gamma / E_{tagged\gamma}$ ,

---

<sup>4</sup>See also Figure 10 (a) in reference [13].

<sup>5</sup>Larger elements lose position information, while smaller elements increase readout costs with little gain in position information.

is approximately 1 for fully contained  $\eta$  decays produced by the golden  $\gamma + p \rightarrow \eta + p$  production channel. Elasticity provides complementary information to the reconstructed invariant mass. While an elasticity cut does not suppress the  $\eta \rightarrow 3\pi^0$  background with photon merging if the  $\eta$ 's were produced by the golden channel, it is the key to removing higher order backgrounds of the “energy imbalance”-type. Examples of events which could pass an invariant mass cut but fail the elasticity cut include 1) pile-up, 2)  $\eta$  production by an untagged off-energy photon coincident with the tagged (but sterile) photon, 3) continuum  $3\pi^0$  production at invariant mass  $> m_\eta$  which migrates down into the  $\eta$  mass window when two photons are lost, or 4)  $\eta$  production by a non-golden channel such as  $\gamma + p \rightarrow \eta + \pi^0 + p$ . The elasticity cut greatly restricts nature’s ability to mimic a signal from a clean  $\eta$  decay.

Simulations were made to compare the expected performance of a  $PbWO_4$  (lead tungstate) and a lead glass calorimeter both in the JEF configuration. The  $PbWO_4$  transverse dimensions were 2.05cmx2.05cm while the lead glass blocks were 4.0cmx4.0cm.<sup>6</sup> Figures 5 and 6 are plots of elasticity versus invariant mass which qualitatively demonstrate the improvement in signal/background expected with  $PbWO_4$ . Because energy and position resolutions are factor of two better in  $PbWO_4$ , the angle and invariant mass resolutions are also about a factor of two better. Projections onto the invariant mass axis in Figures 7 and 8 show the  $\eta \rightarrow 3\pi^0$  background can be suppressed *by about two orders of magnitude* if lead tungstate is used. (Compare also to the invariant mass reconstruction from the Crystal Ball experiment, Figure 4.)

The fact that the remaining background in the lead tungstate calorimeter in Figure 7 is sharply peaked at the  $\eta$  mass indicates is due to photon merging. Obviously, a side-band subtraction would be unreliable, so the remaining  $\eta \rightarrow 3\pi^0$  background must be simulated and subtracted, benchmarked to the huge dataset for  $\eta \rightarrow 3\pi^0 \rightarrow 6\gamma$  we will acquire. On the other hand, loss of photons is not a problem due to our use of boosted  $\eta$ 's.

Another potentially significant background is non-resonant multiple pion production whose reconstructed invariant mass can fall within the  $\eta$  mass window. This is a smooth background so side-band subtractions can be used, but the more we suppress this background, the more sensitive our measurements will be. A Monte Carlo simulation was performed on the  $\gamma p \rightarrow \pi^0\pi^0p$  reaction using PYTHIA. The  $\eta \rightarrow 3\pi^0$  background and  $\eta \rightarrow \pi^0\gamma\gamma$  signal previously presented were added. Figure 9 shows the normalized  $4\gamma$  invariant mass distributions for the  $\eta \rightarrow \pi^0\gamma\gamma$  signal reaction and the two backgrounds. The signal to background ratio is approximately 3:1 which is quite frankly phenomenal. Another study by us has shown the  $2\pi^0$  continuum background can be effectively extinguished, with modest signal losses, by excluding events with two pairs of photons each reconstructing to the  $\pi^0$  mass.

---

<sup>6</sup>The background simulation generated  $\eta \rightarrow \pi^0 2\gamma$  or  $3\pi^0$ , each according to phase space, using PDG relative branching ratios. For events with 4 detected photons, the invariant mass  $M_{4\gamma}$  was calculated with no attempt to build  $\pi^0$ 's at this time. The  $\gamma p \rightarrow \eta p$  cross section is from reference [44].

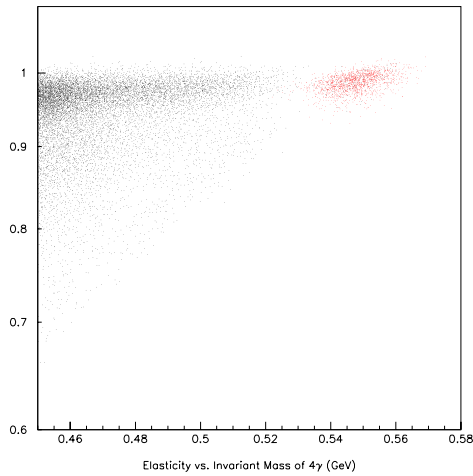


Figure 5: Monte Carlo simulation assuming a  $PbWO_4$  calorimeter in Hall D. The vertical axis is the measured elasticity as defined in the text while the horizontal axis is the reconstructed invariant mass,  $M_{4\gamma}$ . Signal events  $\eta \rightarrow \pi^0\gamma\gamma$  appear as red dots while background  $\eta \rightarrow 3\pi^0$  events are black.

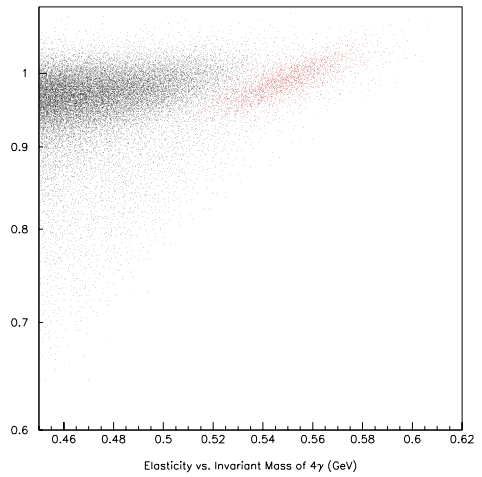


Figure 6: Same conditions as the previous figure but using a conventional lead glass calorimeter.

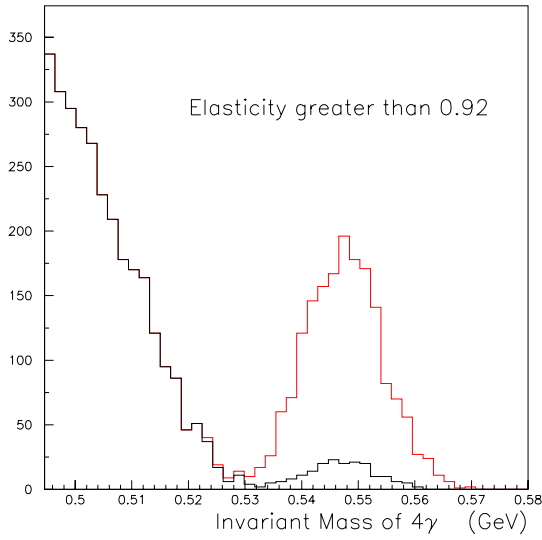


Figure 7: Monte Carlo simulation of  $M_{4\gamma}$  reconstructed in the proposed  $PbWO_4$  crystal calorimeter. The black curve is the background from  $\eta \rightarrow 3\pi^0$  with relative normalization using PDG values. The red curve is the sum of the signal from  $\eta \rightarrow \pi^0\gamma\gamma$  plus background from  $\eta \rightarrow 3\pi^0$ . The signal to background ratio is 7.74. The so-called “peaking background” is due to photon merging.

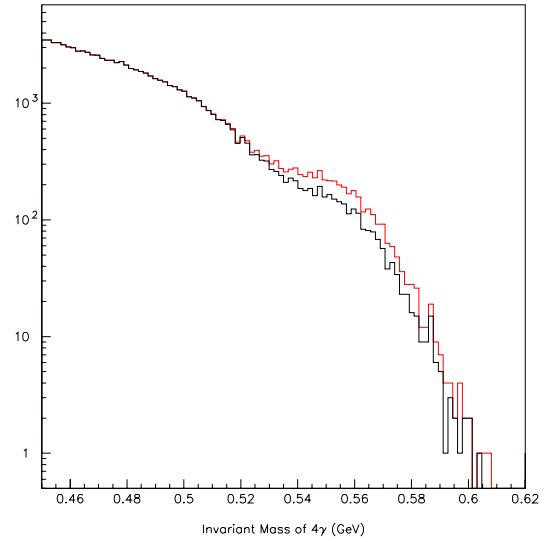


Figure 8: Monte Carlo simulation of  $M_{4\gamma}$  reconstructed from a Pb-glass calorimeter. The black curve is the background from  $\eta \rightarrow 3\pi^0$ . Curves are as in the previous figure. The signal to background ratio is  $8.83 \times 10^{-2}$ .

This means the dominant background in the  $\pi^0 2\gamma$  analysis will be the peaking background seen in Figure 7.

Obviously, the  $\eta \rightarrow 2\pi^0$  search for CP violation cannot exclude events with two pairs of photons each reconstructing to the  $\pi^0$  mass, so the  $2\pi^0$  continuum background is the major limitation to our sensitivity in that analysis. We will use this background to estimate our sensitivity. However, cuts on the recoil proton may help.

EDITOR’S NOTE: REVISE S/B AFTER NEW PLOT WITH HIGHER STATISTICS AND NEW BINNING. (SOMOV)

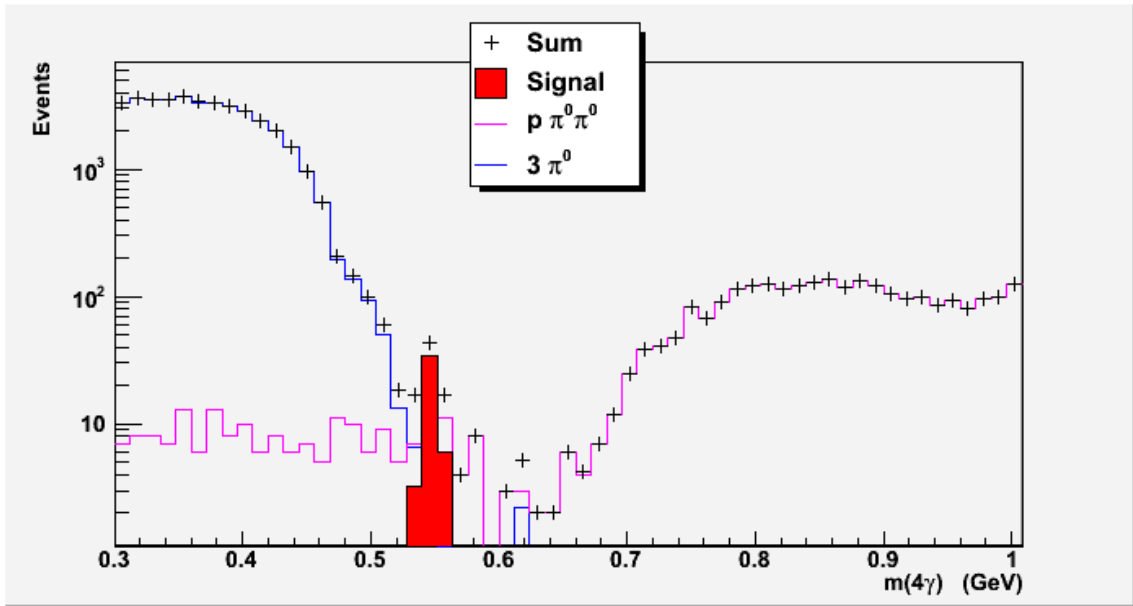


Figure 9: Invariant mass of the  $4\gamma$  distribution including the signal channel  $\eta \rightarrow \pi^0\gamma\gamma$  and both major background channels:  $\eta \rightarrow 3\pi^0$  with missing photons, and continuum  $\gamma p \rightarrow \pi^0\pi^0 p$ . All processes are normalized by estimated cross sections. Signal to background is about 3:1.

The elasticity cut will help suppress  $2\pi^0$  production at little or no cost to our clean  $\eta$  production rate. In forward, high energy  $\eta$  photoproduction by exclusive  $\gamma p \rightarrow \eta p$ , the proton recoil momentum is relatively low because the cross section is dominated by t-channel exchange of a relatively soft virtual photon or light meson. The 3-body background channel  $\gamma p \rightarrow \pi^0\pi^0 p$  on the other hand typically has a larger proton recoil momentum when it involves an s-channel process such as  $\gamma + p \rightarrow \pi^0 + \Delta^+ \rightarrow 2\pi^0 + p$ . The elasticity cut will remove events with more missing energy than can be explained by the  $-t$ -channel  $\gamma + p \rightarrow \eta + p$  production. It will also remove continuum  $3\pi^0$  production with invariant mass greater than  $m_\eta$  which feeds downward into the  $\eta$  mass window after losing 2 photons.

Other aspects of our experiment help suppress backgrounds. Compared to high energy  $\pi^- + p \rightarrow \eta + n$  used by GAMS, our production mechanism does not create an in-time, high energy neutron which could be confused with a gamma ray in the calorimeter. If we detect the recoil proton, which is feasible at our larger  $\eta$  angles, we will be able to verify that the event demonstrates the coplanarity expected for the two-body production channel. Finally, the scintillation in  $PbWO_4$  has a shorter decay time ( $\sim 20$  ns) by about one order of magnitude than NaI(Tl) which helps control pile-up.

One background we probably don't have to worry about is  $\eta \rightarrow 4\gamma$ . Although there are no selection rules which forbid it, it is highly suppressed in the SM and has never been seen ( $BR < 2.8 \times 10^{-4}$ ). No calculation has been published, but the closely related  $\pi^0 \rightarrow 4\gamma$  process has been thoroughly investigated and found to be highly suppressed ( $BR < 10^{-11}$ )[23].

Based on the discussion above, we plan to apply several key techniques in the proposed experiment: (1) the 12 GeV high intensity tagged photon beam in Hall D to produce  $\eta$  mesons on a liquid hydrogen target through the  $\gamma p \rightarrow \eta p$  reaction, (2) a forward high resolution, high granularity  $PbWO_4$  calorimeter to detect multiple-photons from  $\eta$  decays to reduce the  $\eta \rightarrow 3\pi^0$  background, (3) flash ADCs on every crystal for nsec-scale coincidence timing of showers and pile-up rejection, and (4) measuring the recoil  $p$  when feasible with the GlueX detector to suppress non-resonant background from  $\gamma p \rightarrow 2\pi^0 p$  or accidentals.

### 3 Hall D Base Equipment

We propose to use a 9.0–11.7 GeV incoherent tagged photon beam in Hall D to efficiently produce  $\eta$  mesons through the small angle  $\gamma + p \rightarrow \eta + p$  reaction. Multiple decay photons from the  $\eta$ 's will be detected in a new high resolution and high granularity  $PbWO_4$  calorimeter (FCAL-II) located  $\sim 6$  m downstream of the target. When sufficiently energetic, low energy recoil protons will be detected by the start counter and central drift chamber of the GlueX solenoid detector to help suppress backgrounds. As shown in Figure 10, the experimental apparatus includes: (1) a high energy photon tagger; (2) a pair spectrometer for photon flux monitoring; (3) a 30 cm length liquid hydrogen target; (4) the GlueX solenoid detector; (5) an upgraded forward multichannel electromagnetic calorimeter. Except for the calorimeter upgrade and a trigger optimized for detecting  $\eta$  decays, the rest of apparatus is the standard Hall D base equipment. The reference design of the experiment is summarized in Table 2. Details of each instrument are discussed below.

Table 2: Reference design of the JEF experiment.

Parameter	Value
Solenoidal Field	2.2 T
Photon Beam Energy Range	9 - 11.7 GeV
Beam Current	400 nA
Radiator Thickness (Au)	$2 \times 10^{-4} X_0$
5mm Collimator Transmission	30%
Tagged Photon Rate on Target (9-11.7 GeV)	$\sim 4 \times 10^7$ Hz
$LH_2$ Target Length	30 cm (3.46 % R.L.)
$LH_2$ Target Thickness	$1.28 \times 10^{24}$ protons/cm <sup>2</sup>
Cross Section for Forward $\gamma p \rightarrow \eta p$	$\sim 70$ nb
Scintillator in FCAL-II	$PbWO_4$
Outer Active Dimensions of FCAL-II	118cm x 118cm
Beam Hole Dimensions in FCAL-II	12cm x 12cm
Crystal Dimensions	2.05cm x 2.05cm x 18cm
Number of Optically Isolated Crystals	3445
Acceptance of 118 cm x 118 cm FCAL-II	$\sim 20\%$ ( $4\gamma$ ), $\sim 30\%$ ( $3\gamma$ )
Distance Target Center to FCAL-II Front	$\sim 6$ m
Exclusive $\eta$ Production Rate	3.6 Hz (or $3.1 \times 10^5$ /day)
$LH_2$ Production Request	100 days
Total $\eta$ 's Produced in 100 Days	$3.1 \times 10^7$
Effective $\eta$ 's in 100 Days (Includes Acceptance)	$6.2 \times 10^6(4\gamma)$ , $9.3 \times 10^6(3\gamma)$
Total Beam Request	136 days

### 3.1 High Energy Photon Tagger

Hall D is developing and constructing a 12 GeV tagged photon beam line. While details of the design can be found in reference [30], the main features are:

1. Photon energy detection from 70% to 75% of the primary electron beam energy with energy resolution of about 0.5% (r.m.s.) of the primary beam energy. A counting rate of at least  $5 \times 10^6$  electrons per second per 0.1% energy bin over this range of photon energies.
2. Additional capability for photon energy detection from 25% to 97% of the primary electron beam energy. Capable of pre-collimated intensities up to 150MHz/GeV, with 50% sampling of 60 MeV energy bins below 9 GeV and full coverage in 30 MeV wide energy bins above 9 GeV photon energy.

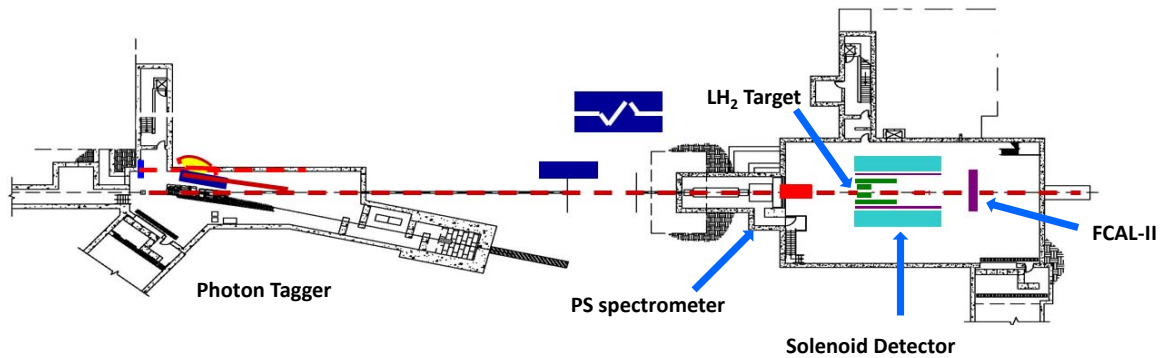


Figure 10: Top view of the experimental setup for  $\eta$  rare decays measurements. This includes: (1) a high energy photon tagger; (2) a pair spectrometer; (3) a solenoid detector with a physics target; (4) a forward  $\text{PbWO}_4$  crystal calorimeter.

The tagging spectrometer is an Elbek-type spectrometer. The 12 GeV electrons pass through the radiator target where a small fraction undergo bremsstrahlung. The electrons then pass through a focusing quadrupole and are bent by the 6 meter long tagger magnet. The majority of the electrons do not significantly radiate and are bent  $13.4^\circ$  to the electron beam dump. A large vacuum vessel is integrated into the magnet and extends to the spectrometer focal plane so the only multiple scattering occurs in the radiator and in the exit window, preserving the resolution. The spectrometer detectors are positioned immediately outside the focal plane to determine the momentum of electrons that produce bremsstrahlung

photons. The photon energy,  $E_\gamma$ , is determined by the difference between the initial electron beam energy and the energy of the post-bremsstrahlung electron deflected towards the focal plane.

The detector package is divided into two parts: (1) a set of 190 fixed scintillation counters spanning the photon energy range from 3.0 to 11.7 GeV, and (2), a movable “microscope” of 500 scintillating fibers optimized for coherent photon beam operation spanning the energy range from 8.3 to 9.1 GeV. The fixed array provides access to the full tagged photon spectrum, albeit at a modest energy resolution of  $\sim 0.1\%$  and reduced rate capability. These detectors are well suited for running with a broadband incoherent bremsstrahlung source. The microscope provides energy resolution better than  $0.07\%$  in order to run in coherent mode at the highest polarization and intensities. Using the microscope, the source is capable of producing collimated photon spectral intensities in excess of  $2 \times 10^8$  photons/GeV, although accidental tagging rates will limit normal operation to somewhat less than this.

For the proposed  $\eta$  rare decays measurement, we will use an incoherent bremsstrahlung photon beam in an energy range from 9.0 GeV to 11.7 GeV. The current design of the fixed scintillation counters in this energy range with 30 MeV wide energy bins is sufficient.

### 3.2 Beam Collimation

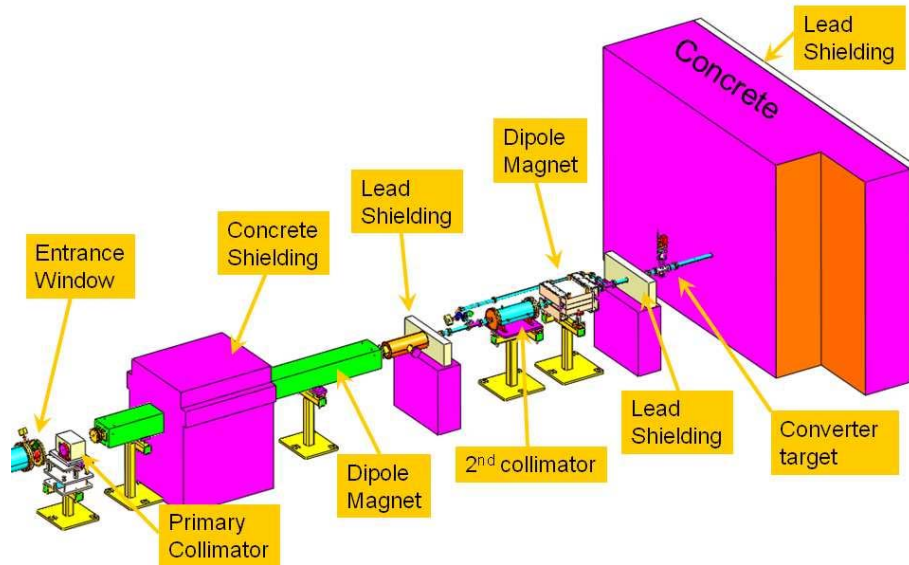


Figure 11: The layout of the collimator cave.

A 12 GeV electron beam interacting with a thin radiator produces the photon beam. The characteristic opening angle for bremsstrahlung photons is  $m_e/E = 42 \mu\text{rad}$ . After 76

meters of drift in vacuum, the photon beam enters the collimator cave from the left through a thin  $250\ \mu\text{m}$  Kapton window  $8''$  ( $203\text{mm}$ ) in diameter and immediately interacts with the primary collimator. The layout of the collimator cave is shown in Figure 11. The primary collimator consists of two main components: an active collimator which measures the centroid of the photon beam and a hybrid tungsten-lead passive collimator. The size of the passive collimator has a couple of options from  $3.4\ \text{mm}$  to  $5.0\ \text{mm}$  in diameter. The active collimator is electrically isolated, has an inner aperture of  $5\ \text{mm}$ , and is precisely mounted in front of the primary collimator. The purpose of the active collimator is to measure the position of the centroid of the photon beam with an accuracy of  $200\ \mu\text{m}$ . The tungsten passive collimator is surrounded by  $8''$  of lead for additional shielding. A large flux of particles are generated in the passive collimator and some lie along the photon beam. A sequence of sweeping magnets after the collimator removes the unwanted charged particles from the photon beam.

A second collimator is located following the lead shielding wall of the first collimator. This collimator is made of stainless steel and is  $20''$  long and  $8''$  in diameter. A  $1\ \text{cm}$  hole is bored along the axis of the collimator and is designed so that the effective aperture can be adjusted to  $6$ ,  $8$ , or  $10\ \text{mm}$  by inserting stainless steel tubes. The purpose of this collimator is to scrape off photons which were produced by small angle scattering on the bore of the primary collimator. A second sweeping magnet is mounted directly after the second collimator. The specification of the tolerance on this alignment during beam operation is a circle of radius  $200$  microns. The size of the beam spot on target is defined by the primary collimator. We plan to use a  $5\ \text{mm}$  diameter primary collimator in the proposed experiment.

### 3.3 Pair Spectrometer and Total Absorption Counter

The most important diagnostics for the photon beam flux are the count rates in the tagger's fixed hodoscope array and the microscope. By detecting the electrons which undergo bremsstrahlung, one determines precisely the energy spectrum of the photon beam in front of the collimators. The photon flux on the target however is only a fraction of the tagged photons because of collimation. The absolute photon flux on the target will depend strongly on the exact details of the collimation. For example, a  $5\ \text{mm}$  diameter primary collimator will pass about  $30\%$  of photons. It is proposed to use pair production, a well understood QED process, as the basis for the relative photon flux determination. An additional calibration measurement is needed to determine the pair spectrometer's absolute efficiency. This is done with dedicated calibration runs at low beam intensity with a total absorption counter (lead glass detector) inserted in the beam after the spectrometer.

The pair spectrometer consists of a thin foil converter ( $1 \times 10^{-3}$  radiation length thick) placed in the photon beam after the last collimator (at  $0.5\ \text{m}$  distance upstream of the front end of the pair spectrometer magnet) to generate electron/positron pairs through pair

production. The electrons and positrons produced in the converter are swept away from the photon beam in a strong dipole field (1.64 T) and are subsequently detected by identical left and right arm detector packages located symmetrically on either side of beam line. The photon energy is then simply the sum of the electron and positron energies. Each detector package covers the electron or positron energy from 3 GeV to 6.25 GeV. It consists of a front detector array for fine position resolution and a back scintillating hodoscope array for fast timing. The back detector array includes 8 scintillator counters mounted up and down alternatively with 2 mm overlap on either side. Each counter is made from plastic scintillator with dimension of 4.4 cm wide, 2.0 cm thick, and 6.0 cm long. It is glued to a 16 cm long fish-tail light guide from one end then coupled to a 1" PMT. The back detector is designed to provide 200 ps time resolution to form the pair production trigger.

The proposed experiment will use the incoherent photon beam at the highest possible energy ( $E_\gamma=9\text{--}11.7$  GeV). We will measure the branching of various rare decays by normalizing to the  $\eta \rightarrow \gamma\gamma$  channel. The design specifications for the pair spectrometer is to monitor the beam flux at  $\sim 1\%$  level, which is better than needed for the proposed experiment.

### 3.4 Target

We propose to use the standard Hall D liquid hydrogen target with 30 cm length, corresponding to approximately 3.46% radiation lengths. Hall D is planning to use a cryogenic target system similar to what has been developed for Hall B [31]. While some details of the Hall D target system are still undefined, the main element of the cryogenic target is a heat exchanger in contact with the target that is refrigerated down to 2.5 K by pumping liquid helium through a Joule-Thompson valve. Experience in Hall B has shown that after a 15-liter buffer cryostat has been filled from the torus, oscillations in the target temperature are smaller than  $\pm 0.02$  K [32]. The Hall B g10a target cell, with design similar to that proposed for use in Hall D, is 24 cm in length. The upstream end of the target has an inner diameter of 5.51 cm, tapering down to 4.0 cm inner diameter on the downstream end of the target. The reason for the taper is to eliminate dead zones in the target, where cooling is limited. The radius on the endcaps is 4 cm. The target cell is constructed from 5 mil kapton.

During the proposed experiment, target temperatures and pressures will be written into the data stream. Since significant target heating does not occur for a real photon beam, the target density can be deduced from the equation of state and the target pressure-temperature data. However, as we are measuring a branching ratio rather than an absolute cross section, we are insensitive to changes in target density.

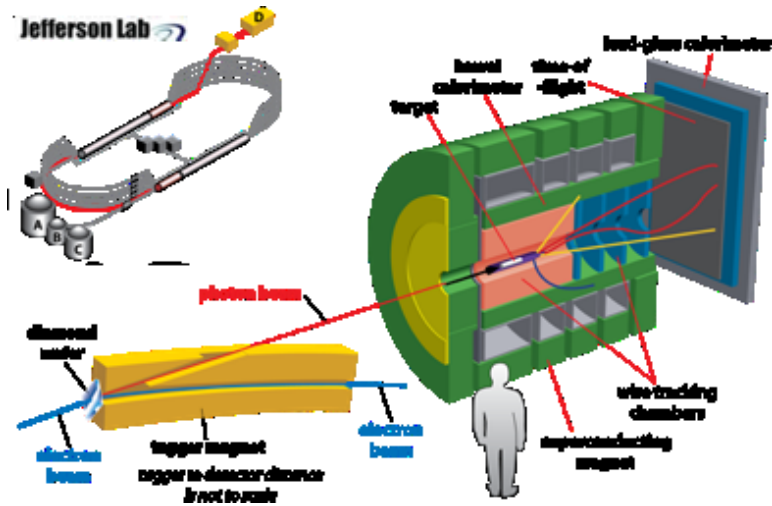


Figure 12: The cross-sectional view of the complete original GlueX detector. The apparatus is detailed in detail in Section 3.5.

### 3.5 The Gluex solenoidal detector

The photon beam used in this experiment will be produced in the tagger hall and travel 76 m, after which the beam will pass through a collimator. The photons then interact in a liquid-hydrogen target. Outside the target, there is a scintillator-based start counter, the central drift chamber (CDC), and the lead scintillating fiber barrel calorimeter (BCAL) all inside a 2.2 T solenoid [35]. Most particles exiting the solenoid in the forward direction will strike a time of flight (TOF) wall. The complete GlueX apparatus is depicted in Figure 12.

#### 3.5.1 Solenoid

The solenoid magnet creates a 2.2 T magnetic field at the center of the magnet oriented parallel to the beamline [36]. The magnet is 4.65 m long, has an inner diameter of 2.03 m, and an outer diameter of 3.76 m. The self inductance of the coil is 26.2 H hence at the nominal current of 1500 A the stored energy is 29.5 MJ. The solenoid consists of 4 separate superconducting toroidal coils and cryostats and was recycled from previous experiments.

The superconductor is a composite twisted multi-filament wire made of niobium-titanium. The wire is made by soldering the superconductor composite between two copper strips to form a rectangular cross section ( $0.763 \times 0.533 \text{ cm}^2$ ) which is wound on the inner wall of the cylindrical liquid helium vessel. Along with the composite, strips of 0.025" thick stainless steel, for structural support, and two 0.0075" Mylar strips, for insulation, were also included.

### 3.5.2 Central Drift Chamber (CDC)

The Central Drift Chamber (CDC) consists of 3500 1.5 m long straw tubes [38]. The straws are oriented in two directions: axial (12) and stereo (16), in order to provide better spatial resolution in the z or longitudinal coordinate. The CDC is a large cylinder surrounding the target and start counter with an inner radius of 20 cm and an outer radius of 120 cm. The expected position resolution of the CDC is 150  $\mu\text{m}$ . For the nominal position for the  $LH_2$  target, the angular coverage of the CDC is  $6^\circ$  to  $165^\circ$ .

The CDC gives us the option of detecting recoil protons.

### 3.5.3 Start Counter

The start counter is barrel hodoscope consisting of 40 scintillators surrounding the target that will be used, in conjunction with the tagger, to measure the beam bucket of the associated event [37]. The detector is a 50 cm long cylinder with a 10 cm cone that tapers toward the beamline on the downstream end of the target. The start counter accepts charged particles at angles between  $3^\circ$  and  $134^\circ$  over the full length of the target. The start counter is self-supporting as to not introduce additional material in the path of the particles.

The start counter will be useful in flagging the presence of extra charged particles, and for recoil protons will provide large pulses with good timing resolution.

### 3.5.4 Barrel Calorimeter (BCAL)

The barrel calorimeter (BCAL) is a lead-scintillating fiber sampling calorimeter that lines the inside of the solenoid. Each individual module consists of layers of corrugated lead sheets, interleaved with planes of 1 mm, round, Kuraray SCSF-78MJ scintillating fibres, bonded to the lead grooves using optical epoxy [39]. The complete detector will consist of 48 identical wedge-shaped modules with each module occupying  $7.5^\circ$  of azimuthal angle. Each module is 3.9 m long and 22.46 cm thick, and once assembled into the final ring shape, the BCAL will have an inner radius of 65 cm and an outer radius of 90 cm. The entire BCAL, readout included, resides within the 2.2T magnetic field and will be read out by about 4,000 field-insensitive large-area ( $1.26 \text{ cm}^2$  each) silicon photomultiplier arrays.

The BCAL will be used to flag the presence of any extra gamma rays.

### 3.5.5 Time of Flight (TOF)

The time of flight (TOF) detector wall is an array of 2.54 cm thick and 6 cm wide scintillator paddles [40]. The paddles are read out on each end by XP2020 PMTs, except in the middle where the beamline only allows single ended readout. There will be a horizontally oriented wall and a vertically oriented wall to provide additional location information for a total of 84 paddles. The TOF detector will cover angles of  $1^\circ$  to  $11^\circ$ , providing an overlap with the start counter of angles  $3^\circ$  to  $11^\circ$ . The primary purposes of the TOF detector are to determine charged track multiplicity and provide excellent TOF information with respect to an RF bucket.

## 4 FCAL-II Setup and Low-Level Reconstruction

The  $\eta$  signal is primarily identified by reconstruction of the invariant mass,  $M^2 = p^2 \equiv (\Sigma E_\gamma, \Sigma \vec{P}_\gamma)^2$ , from the summed 4-momenta of the decay photons detected in the forward multi-channel calorimeter. The relative error in invariant mass reconstruction is approximately given by the quadrature sum of the relative errors in energy and angle. We require percent-level resolution in shower energy reconstruction and, given a typical shower opening angle of 10's of cm, mm-scale resolution in calorimeter hit position to determine the angle of the photon.

To minimize shower merging and pile-up in the calorimeter, high granularity and fast decay time are also critical. The scintillator  $PbWO_4$  has highly desirable properties for use in an electromagnetic calorimeter, including a small Molière radius (2.1 cm), short radiation length (7.4 g/cm<sup>2</sup>), and fast decay time (30 ns). It is also highly radiation resistant and available in large quantities. Based on these features, and the extensive experience of some of us with a smaller lead tungstate calorimeter employed in the PrimEx experiment, we propose to use  $PbWO_4$  crystals in an upgraded Hall D Forward Electromagnetic Calorimeter (FCAL-II).

Finalizing the ultimate size of the calorimeter will involve a trade-off between acceptance and cost. For a tagged photon beam of 9.0–11.7 GeV, the average acceptance for 4 photons in the  $118 \times 118$  cm<sup>2</sup> calorimeter is  $\sim 20\%$  while that of the  $150 \times 150$  cm<sup>2</sup> version is  $\sim 40\%$ . (See Figure 23 for the 3 photon acceptance and Figure 24 for the 4 photon acceptance.) In keeping with our philosophy of bridled enthusiasm, all projections in this proposal are based on the smaller, lower acceptance (and lower cost) calorimeter. However, it's worth noting that for less than 60% additional cost, the larger version of the calorimeter would increase the 3-4 $\gamma$  acceptance an average of 80% while simultaneously reducing the fraction of  $\eta \rightarrow 3\pi^0$  events with lost photons.

Our design is basically a larger version of the lead tungstate core of the PrimEx HyCal calorimeter, a 59 element x 59 element matrix of optically-isolated crystals each of size  $2.05 \times 2.05 \times 18 \text{ cm}^3$ . The crystal transverse dimensions of  $2.05 \times 2.05 \text{ cm}^2$  are comparable to the Molière radius of lead tungstate so that shower energy sharing between adjacent crystals can be used to determine the position of the shower with mm-scale accuracy at the energies of interest. The 18 cm thickness (20 radiation lengths) has been shown by PrimEx to be sufficient to achieve the required energy resolution. A central  $\sim 12 \times 12 \text{ cm}^2$  hole will be left open to enable the photon beam and small angle electromagnetic background to pass downstream.

Scintillation light from the electromagnetic shower will be detected with Hamamatsu R4125HA photomultiplier tubes coupled to the back of the crystals with optical grease. A fiber optic cable will be glued to the front face of each module for the gain monitoring system. If instrumented as in the PrimEx HyCal, there will be a HV and two signal cables for each base (one for the anode and another for the dynode). The anode signals will each go to a flash ADC as discussed below. The dynode signals will be summed first in groups, and then groups will be summed to form a total calorimeter energy signal for use in the trigger and to provide a hardware timing reference.

An exciting development in JLab's 12 GeV era is the standardization of most new detector readout systems to flash ADCs. By keeping the cost per channel to less than \$300 (and the loaded cost per channel including VME crate, CPU, etc. to less than \$400), a single channel of 12 bit, 250 MHz flash ADC (plus fairly cheap memory and processing power) can substitute for an older non-flash ADC, a TDC, and two delay lines. This saves money, space, procurement time, and labor. Sampling is continuous and deadtimeless. When a shower occurs, the 4 nsec samples will be recorded so that the pedestal (zero offset), the energy, and the time can be determined offline. Tests indicate the time resolution is better than 1 nsec[41]. This will allow us to constrain all photons in the event to the same beam burst and so minimize accidental coincidences. Flash ADCs are not merely cost-effective substitutes for older technology, they have been used in rare decay experiments for decades because they allow one to sensitively flag pile-up and even scrutinize interesting events individually when desired. The combination of  $PbWO_4$  crystals and a flash ADC on each channel will make FCAL-II truly a cutting edge calorimeter for the 21st century.

Several institutions on this proposal are also major players in the PrimEx collaboration and were heavily involved in the design and construction of the state-of-the art, high resolution,  $PbWO_4$  crystal and Pb glass Hybrid Calorimeter (HyCal). That detector was used in both the PrimEx-I and PrimEx-II runs. Their experience will be very important for successfully realizing FCAL-II in Hall D. In the next section, we will discuss the performance of the  $PbWO_4$  calorimeter in the PrimEx-I and PrimEx-II experiments.

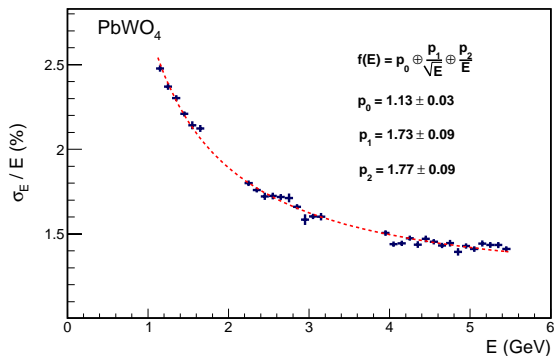


Figure 13: Measured result for the  $PbWO_4$  calorimeter energy resolution *versus* initial incident photon energy. (PrimEx-I calibration) Extrapolated to 10 GeV, the energy resolution will be 1.3% or 130 MeV.

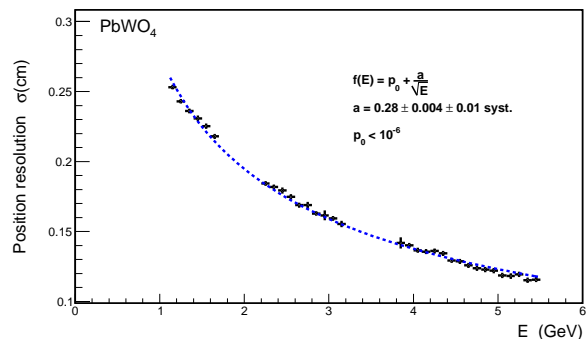


Figure 14: Measured result for the  $PbWO_4$  calorimeter position resolution *versus* initial incident photon energy. (PrimEx-I calibration) Extrapolated to 10 GeV, the position resolution will be 0.9mm.

#### 4.1 Energy and Position Resolutions in the PrimEx $PbWO_4$

During the PrimEx-I experiment in 2004, calibration of HyCal was performed using a low intensity tagged photon beam with energies of  $E_\gamma = 0.5 - 5.5$  GeV. After the center of each detector module was irradiated, the calorimeter was moved to scan the photon beam continuously across entire front face of the calorimeter, row by row. The measured energy and position resolutions *versus* initial incident photon energy are shown in Figure 13 and Figure 14 respectively. Excellent energy and position resolutions were achieved, crucial to achieving good resolution in  $M_{\gamma\gamma}$  needed to isolate good  $\pi^0$  events from background and to accurately determine the  $\pi^0$  production angle used to identify the Primakoff peak. A 2.8% total uncertainty on the  $\pi^0$  lifetime [42] was obtained in PrimEx-I, a factor of two and half more precise than the Particle Data Group average of several old experiments [43].

The PrimEx program proved the  $PbWO_4$  material to be highly radiation resistant. In terms of angle, the central beam hole in HyCal was more than 3x smaller than we plan for FCAL-II in Hall D ( $4.1 \times 4.1$  cm<sup>2</sup> at 7 m for Hycal versus  $16 \times 16$  cm<sup>2</sup> at 6m for FCAL-II). HyCal was in the beam for more than three months at  $7 \times 10^7$   $\gamma$ 's/sec on a 5% radiation length (R.L.) target during PrimEx-I and a 10% R.L. target in PrimEx-II. When calibration data were compared from the beginning and end of the program, the gain changes for  $\sim 1200$  channels were less than a few percent.

## 4.2 Pile-Up in the PrimEx $PbWO_4$

Another important issue in calorimetry is pile-up, the probability that any given event will appear in combination with clusters from a separate scattering in the target. In our rare-decay experiment, pile-up could cause  $\eta \rightarrow 2\gamma$  events to look like  $\eta \rightarrow 3\gamma$  events, or it could push  $\eta \rightarrow 3\pi^0$  events with lost photons back into the elasticity cut. During both PrimEx-I and PrimEx-II, clock trigger events were used to open a 100 nsec wide ADC gate with no bias. Figure 15 and Figure 16 show the energy-dependent occupancy seen by PrimEx-II, the green points with 100 MeV threshold being most relevant. Although the analysis of the PrimEx-II dataset is still ongoing, integration of the green points suggests that pile-up probability for the array will be about 1%.

This very modest 1% PrimexII pile-up probability for a 100 MeV threshold is extremely encouraging.<sup>7</sup> First of all, the use of Flash ADCs will allow us to determine the time of each energy deposit and reject those events, reducing the pile-up contamination to  $1 \times 10^{-4}$ . This is more than sufficient to keep the  $\eta \rightarrow 3\pi^0$  background with missing photons under control. Secondly, increasing our minimum photon cluster energy to 360 MeV would not only reduce pile-up another factor of 2, it would allow the elasticity cut at high confidence to reject an extraneous hit would could cause  $\eta \rightarrow 2\gamma$  to mimic  $\eta \rightarrow 3\gamma$ .

## 4.3 photon merging in a cluster reconstruction algorithm

Recently, collaborator I. Larin developed a so called “Island Algorithm” for cluster reconstruction in the calorimeter to improve the efficiency of shower reconstruction and minimize overlapping showers. We discuss it here because it is relevant to the background in the  $4\gamma$  channel due to photon merging from the large branch  $\eta \rightarrow 3\pi^0$ .

The algorithm follows three steps: (1) identifying a crystal cell with the maximum energy deposition; (2) declaring all surrounding connected cells as an initial “raw” cluster; (3) splitting the “raw” cluster into many hits based on the transverse shower profile function. The transverse shower profile function for the  $PbWO_4$  crystal was measured with a  $6 \times 6$  matrix  $PbWO_4$  prototype detector in a secondary electron beam. The  $x$  and  $y$  coordinate of incident beam were determined by a scintillating fiber detector located in front of the prototype calorimeter. The scintillating fiber detector consisted of two scintillating fiber arrays with a 0.6 mm resolution. Figure 17 shows the experimental result for a 2-dimensional shower profile, and Figure 18 shows the shower profile function extracted from the experimental data in Figure 17.

---

<sup>7</sup>The comparison isn’t completely apples to apples, since the calorimeter size, beam hole size, and beam energy are different between PrimEx-II and JEF, but factors of several do not matter in this discussion.

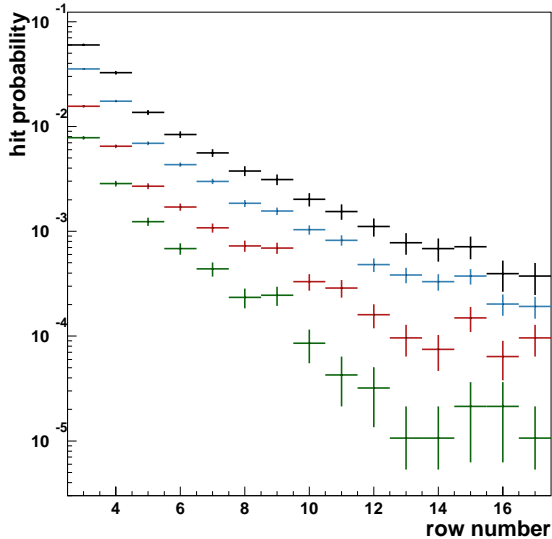


Figure 15: Probability of a row of crystal modules to register a hit *versus* the row number counting from the beam axis. (PrimEx-II data) Since there is a square beam hole, the first row begins at 3. The black, blue, red and green data points are for the energy deposits in the counter greater than 10 MeV, 20 MeV, 50 MeV, and 100 MeV, respectively. The green points with 100 MeV threshold are most relevant.

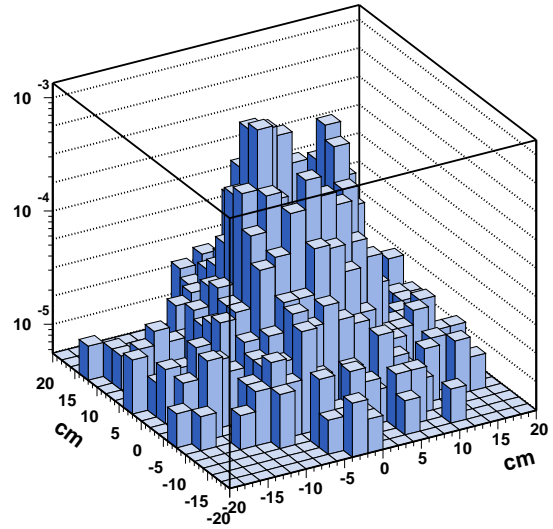


Figure 16: The  $\gamma$  occupancy probability distribution on the HYCAL measured in PrimEx-II.

This newly developed cluster reconstruction algorithm was tested by mixing two hits from the PrimEx-II “snake scan” data. A 5 GeV hit was selected from the data as the stationary shower, while a second hit with energy of 1–5 GeV approached the stationary one. The “Island Algorithm” was applied to reconstruct the clusters. Any cases where the two hits were reconstructed as a single cluster were counted as inefficient.

Figure 19 and Figure 20 are the resulting two-cluster reconstruction efficiency *versus* the separation distance between two hits for the  $PbWO_4$  and conventional Pb glass, respectively. There is no merging of clusters in the  $PbWO_4$  calorimeter when the showers are separated by at least 2.5cm, and the majority of close showers are identifiable as such even when their axes are as close as 1.25cm. In lead glass, showers begin to merge even when hits are separated by 6cm, although the majority of close showers can still be flagged as two hits when they are as close as 4.25cm. Using the separation at which 50% of two-cluster hits are reconstructed

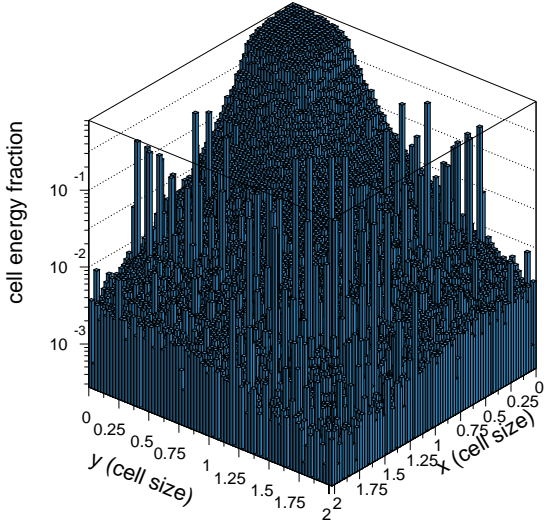


Figure 17: The  $PbWO_4$  calorimeter transverse shower profile measured from the PrimEx beam test.

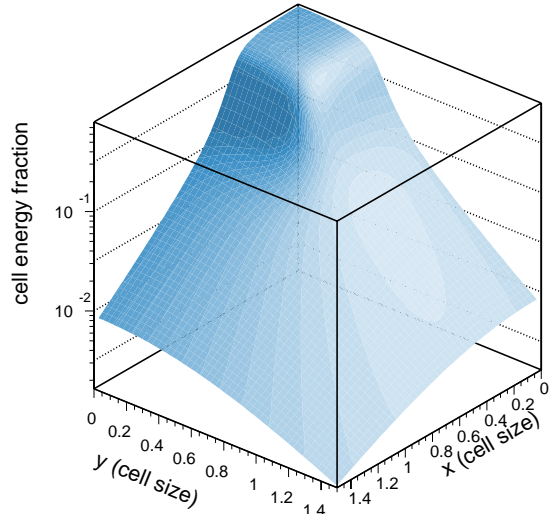


Figure 18: The  $PbWO_4$  calorimeter transverse shower profile distribution function extracted from the PrimEx beam test result shown in Figure 17.

as a single hit, the use of lead tungstate can be expected to reduce merging probability by roughly  $(4.25cm/1.25cm)^2 \sim 12$ .

#### 4.4 trigger and data acquisition

EDITOR'S NOTE: PUT SOMETHING HERE REFLECTING OUR RELATIVELY LOW TRIGGER RATES WHILE KEEPING IN MIND THAT OFFLINE FLAGGING OF PILE-UP REQUIRES WE KEEP 50-100 NSEC OF FLASH ADC SAMPLES FOR CHANNELS ABOVE PEDESTAL (SOMOV)

## 5 FCAL-II Acceptance and High-Level Reconstruction

$\eta$  rare decay events will be reconstructed from FCAL-II information, normalizing to  $\eta \rightarrow \gamma\gamma$  decays measured simultaneously. Since our goal is to measure the branching ratios,

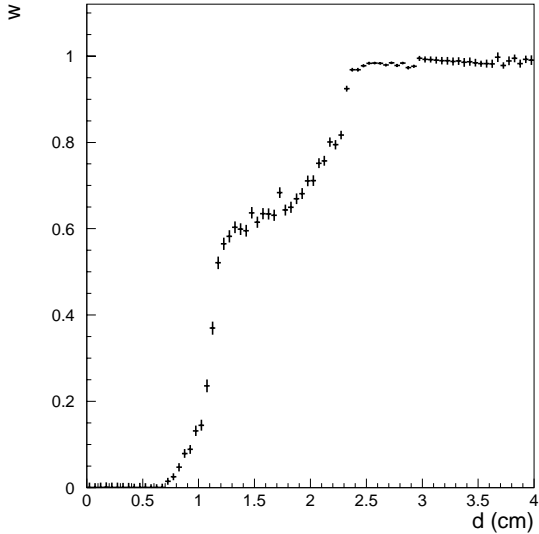


Figure 19: The  $PbWO_4$  calorimeter two-cluster reconstruction efficiency *versus* the separation distance between two showers.

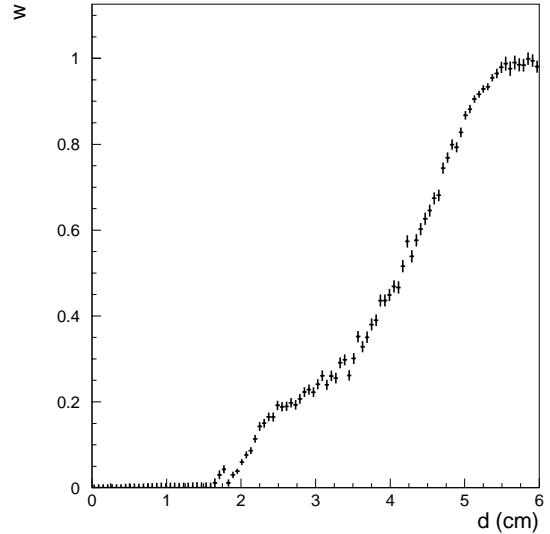


Figure 20: The Pb glass calorimeter two-cluster reconstruction efficiency *versus* the separation distance between two showers.

knowledge of the absolute luminosity and detection efficiency are important but not as critical as in the PrimEx program where absolute decay widths are determined. Our priorities are isolation of the signal with high efficiency while minimizing the background, specifically, optimizing the figure of merit  $N_\eta \times Acceptance / \sqrt{N_{bkg}}$ . To achieve this goal, one needs (1) the geometrical acceptance for each  $\eta$  decay channel under study, (2) effective cut parameters and their resolutions.<sup>8</sup>

## 5.1 calorimeter geometrical acceptance

Geometrical acceptance for a given  $\eta$  decay largely depends on the usual suspects in any solid angle: the distance between the target and FCAL-II, and the effective frontal area of FCAL-II. But it also decreases with increasing number of photons since there are more opportunities to lose a photon down the beam hole or (more importantly) around the outer edges of the calorimeter.

Two flagship channels for our experiment are the  $4\gamma$  final states,  $\eta \rightarrow \pi^0\gamma\gamma$  and  $\eta \rightarrow$

---

<sup>8</sup>For this discussion, we will assume the signal is extracted from a series of cuts rather than a single cut on a likelihood parameter.

$\pi^0\pi^0$ . As discussed earlier, one of the most critical backgrounds for rare  $\eta$  decays leading to  $4\gamma$ 's comes from the apparent merging of photons in the calorimeter from  $\eta \rightarrow 3\pi^0$ . For fixed calorimeter size, as the distance between the target and calorimeter is varied, there is a trade-off between signal and the photon merging background. To optimize this distance, we employ the figure-of-merit (FOM)  $FOM \equiv S/\sqrt{B}$  where  $S$  is the number of  $\eta \rightarrow \pi^0\gamma\gamma$  events detected, and  $B$  is the number of background events from  $\eta \rightarrow 3\pi^0$  within a  $\pm 3\sigma$  window around the  $\eta$  invariant mass. Figure 21 shows this FOM as a function of distance.

Unless otherwise specified, all acceptances are reported for the reference design of  $118 \times 118 \text{ cm}^2$  at the “ $4\gamma$ ” plateau near 6 m, and for the beam energy range of 9-11.7 GeV. For  $\eta$  decays into  $2\gamma$ ,  $3\gamma$ , and  $4\gamma$  final states, the geometrical acceptances are given by Figures 22, 23, and 24, respectively. The average acceptance is  $\sim 45\%$  for  $2\gamma$ ,  $\sim 30\%$  for  $3\gamma$ , and  $\sim 20\%$  for  $4\gamma$  final states. For the larger,  $150 \times 150 \text{ cm}^2$  calorimeter, the acceptance in each case increases by 0.2 which would approximately double the  $4\gamma$  acceptance.

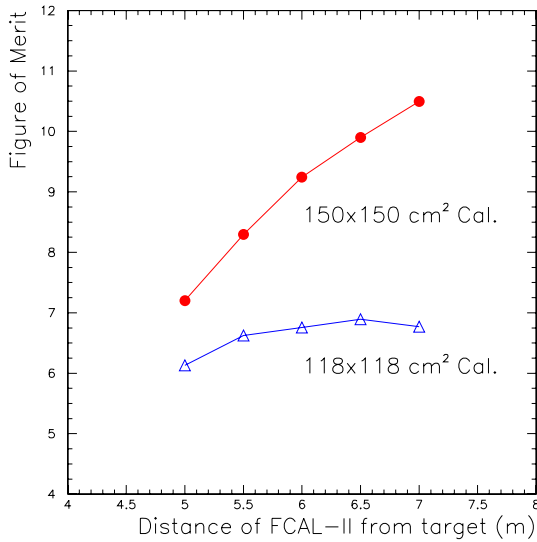


Figure 21: The figure-of-merit  $S/\sqrt{B}$  versus the distance between target and FCAL-II, where  $S$  is the accepted  $\pi^0 2\gamma$  signal and  $B$  is the background from photon merging in  $\eta \rightarrow 3\pi^0$  decays which have a branching ratio 3 orders of magnitude larger. The reference design of  $118 \times 118 \text{ cm}^2$  is plateaued near 6m.

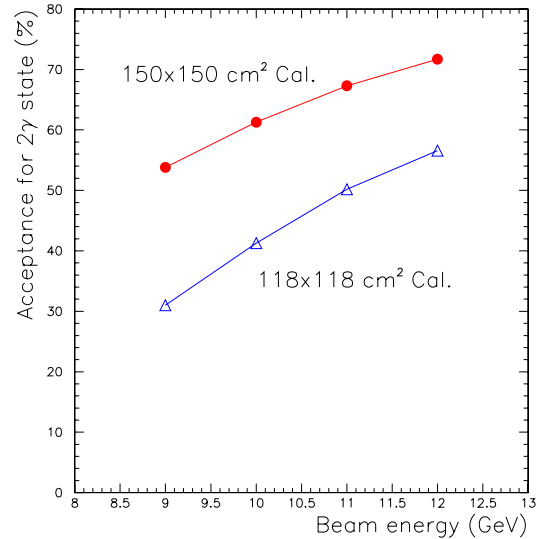


Figure 22: The geometrical acceptance for  $\eta \rightarrow \gamma\gamma$  versus the beam energy. This is our normalization channel.

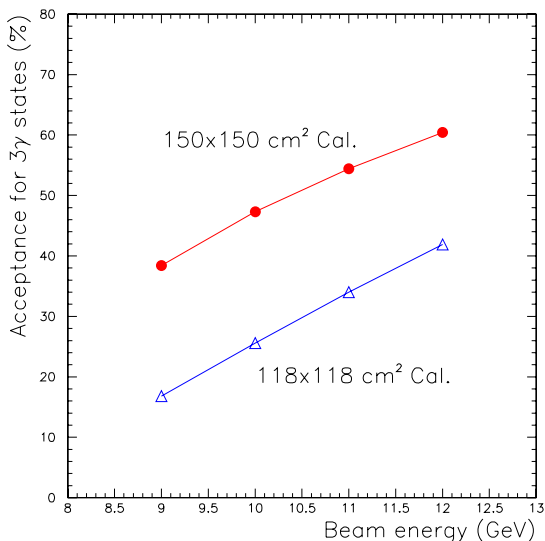


Figure 23: The geometrical acceptance for the  $3\gamma$  states ( $\eta \rightarrow 3\gamma$  or  $\eta \rightarrow \pi^0\gamma$ ) versus the beam energy. These are the channels used to search for new sources of C violation.

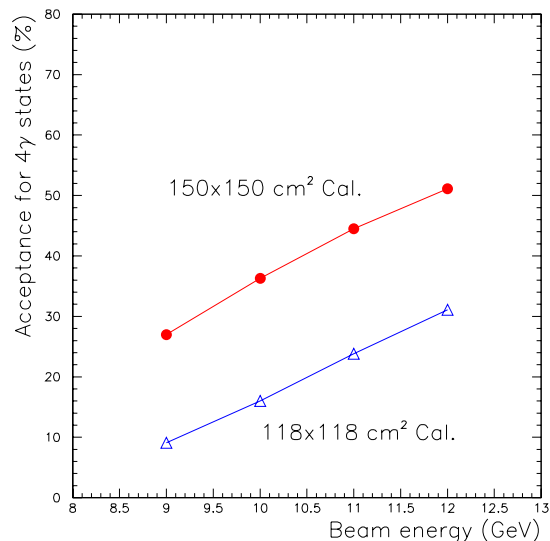


Figure 24: The geometrical acceptance for the  $4\gamma$  states ( $\eta \rightarrow \pi^0\gamma\gamma$  or  $\eta \rightarrow \pi^0\pi^0$ ) versus the beam energy. This is the channel used to search for new sources of P and CP violation.

## 5.2 calorimeter resolutions in elasticity and invariant mass

There are two major kinematical variables for selection of  $\eta$  decays events. The first is the elasticity—the ratio of total energy deposited in FCAL-II to the tagged photon beam energy. Resolution in elasticity depends on the calorimeter energy resolution and, to a lesser extent, the tagger energy resolution. The second variable is the particle’s invariant mass reconstructed from the decay of 2 or more photons. In both cases, energy resolution is important, but for the invariant mass the angle resolution is also critical. Since no tracking is possible with photons, the photon angle is determined by the hit position on the calorimeter and the target position. The beam is transported almost entirely in vacuum so the vast majority of high energy calorimeter triggers arise from the target.

Simulations were performed assuming the proposed  $PbWO_4$  crystal calorimeter and generating  $\gamma + p \rightarrow \eta + p$  events along the length of a 30 cm  $LH_2$  target. No information about the recoil proton was used in the reconstruction. Figure 25 shows the resolution in the elasticity variable for fully contained  $\eta \rightarrow \pi^0 2\gamma$  decays. Resolutions for  $2\gamma$  and  $3\gamma$  final states are similar. The average peak position is slightly less than 1 due to the missing energy carried away by the proton recoil. Assuming a typical photon energy of 10 GeV,

the elasticity resolution of 0.012 corresponds to a missing energy sensitivity of 120 MeV. This cut virtually ensures the forward neutral meson production (be it a  $\pi^0$ ,  $\eta$ ,  $\phi$ , etc.) was exclusive even without recoil proton detection. It is barely possible for a very soft additional  $\pi^0$  to slip past this cut, but the resulting extra photons would have little or no acceptance in FCAL-II while having good acceptance in BCAL, and would be below the energy threshold for shower reconstruction in FCAL-II in any case.

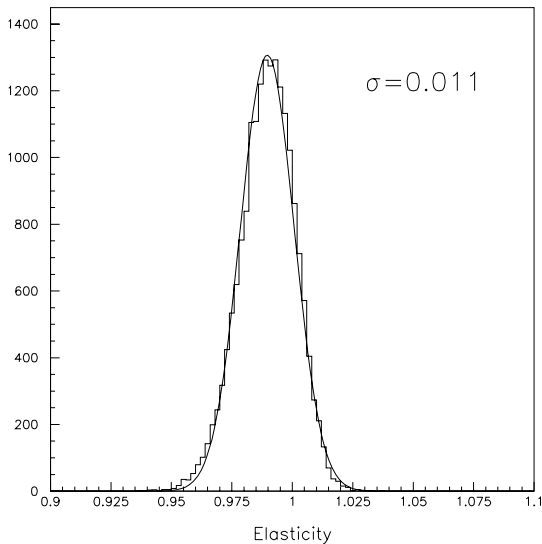


Figure 25: Elasticity for  $\eta \rightarrow \pi^0\gamma\gamma$ . The resolutions for  $\eta \rightarrow 2\gamma$  and  $\eta \rightarrow 3\gamma$  are similar, 1.3% and 1.2%, respectively.

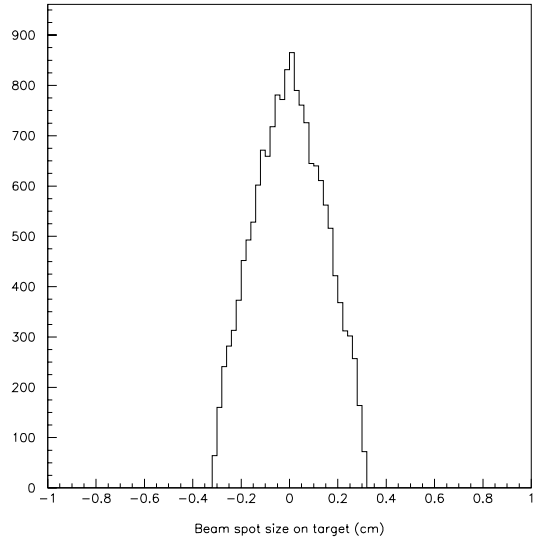


Figure 26: The  $x$  (transverse) distribution of the interaction vertices in the target for a 5 mm diameter primary collimator. The rms width of less than 0.2cm makes a much smaller contribution to the invariant mass resolution than does the calorimeter energy resolution.

The resolution in invariant mass arises from several factors: (1) the photon beam spot size on the target, (2) the uncertainty of the reaction vertex along the target length if the recoil proton is not detected (as in the simulations presented here), (3) the energy and position resolutions of FCAL-II, and (4) the energy of the photons detected by the calorimeter. The size of the beam spot is directly correlated with the size of the primary collimator in the beam line. For illustration, Figure 26 shows the beam spot  $x$  (transverse) projection on the target for a 5 mm diameter primary collimator. In order to simulate the invariant mass resolutions, we have taken into account the beam spot size with a 5 mm diameter primary collimator, a 30 cm thick  $\text{LH}_2$  target, 6 m distance between the FCAL-II and the target, and a photon beam in the energy range of 9-11.7 GeV. Because the recoil

proton was not required in this simulation, reconstruction assumed all events arose from the target center.

The reconstructed  $\eta$  invariant mass resolution for the  $\eta \rightarrow \pi^0\gamma\gamma$  reactions is shown in Figure 27. Resolutions for  $2\gamma$  and  $3\gamma$  final states are similar. Despite the high photon energy, the average rms resolution of 11 MeV in is only 2% of the  $\eta$  mass. This is our most important cut to select  $\eta$  decay signals while suppressing continuum backgrounds. It will also be used to identify  $\pi^0$ 's,  $\phi$ 's, etc., for calibration as well as physics initiatives beyond the scope of this proposal.

Figure 28 shows that the invariant mass resolution of the  $\pi^0$  from the  $\eta \rightarrow \pi^0\gamma\gamma$  reaction is 3.8 MeV. The importance of the  $\pi^0$  resolution will be discussed in the next section on event selection. The resolution can be improved an additional 35% using kinematical fits [46][47].

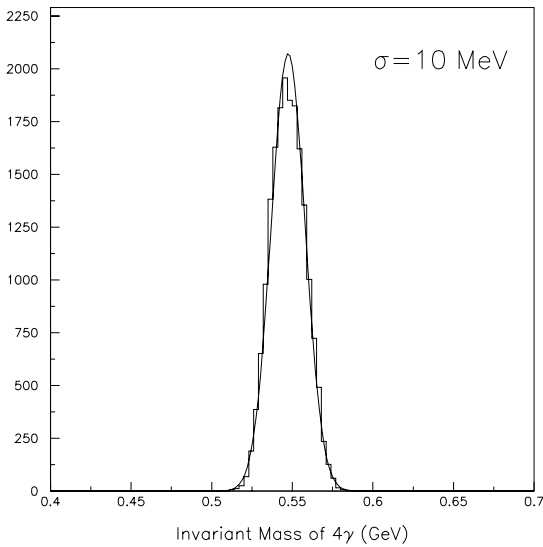


Figure 27: Reconstructed invariant mass  $M_{4\gamma}$  from the  $\eta \rightarrow \pi^0\gamma\gamma$  reaction. The resolution for  $2\gamma$  and  $3\gamma$  final states is similar, 12 MeV and 11 MeV, respectively.

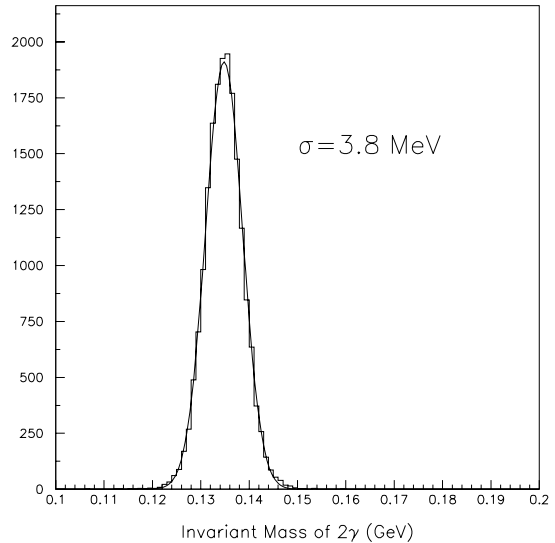


Figure 28: Reconstructed invariant mass  $M_{2\gamma}$  of the  $\pi^0$  from the  $\eta \rightarrow \pi^0\gamma\gamma$  reaction.

### 5.3 basic event selection

Event selection begins at the trigger level. For 9-11.7 GeV photon beam proposed in this proposal, Figure 29 shows the distribution of the energy deposited in FCAL-II from the

exclusive reaction  $\gamma p \rightarrow \eta p$ , followed by  $\eta \rightarrow \pi^0 \gamma \gamma$ . Plots for  $\eta \rightarrow 2\gamma$  and  $\eta \rightarrow 3\gamma$  (not shown) look very similar. Figure 30 shows the total energy spectrum in FCAL-II for one of the major inelastic reactions,  $\gamma p \rightarrow \eta \pi^0 p$ . As one can see, for the beam energy in 9–11.7 GeV range, an FCAL-II threshold of about 8 GeV would safely select all signal events while suppressing triggers from inclusive production or accidental beam related background. The elasticity cut mentioned below performs a more detailed comparison of tagged photon energy and total calorimeter energy.

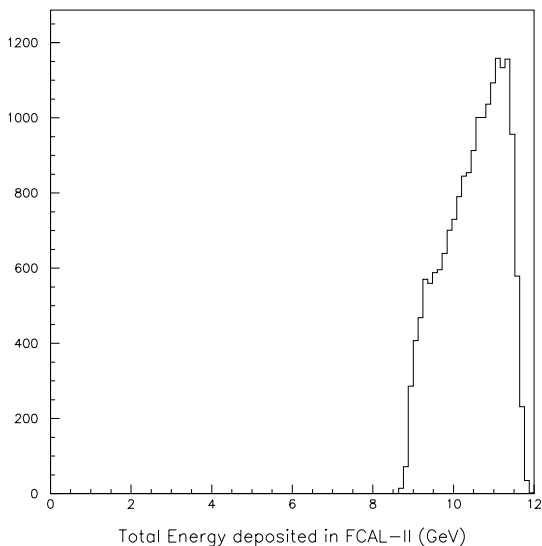


Figure 29: Reconstructed total energy deposited in FCAL-II by  $\eta \rightarrow \pi^0 \gamma \gamma$ . Nearly all events of interest deposit more than 8.5 GeV in the calorimeter (modulo the energy resolution, this is simply explained by the minimum photon beam energy of 9 GeV less the sum of the  $\eta$  mass and proton recoil energy).

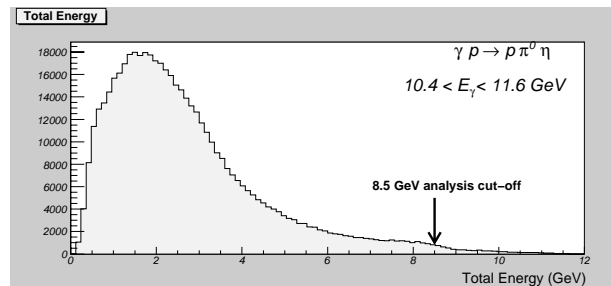


Figure 30: Total energy deposited in FCAL-II by inelastic  $\eta$  production through the  $\gamma p \rightarrow \eta \pi^0 p$  reaction.

In the offline analysis, we will apply the following basic event selection criteria for tagged photon energies of 9–11.7 GeV: (0) single hit in the tagger for 9–11.7 GeV; (1) fiducial volume of FCAL-II for full shower containment (i.e., excluding the inner and outermost layers of crystals); (2) every shower in a candidate neutral meson must have good coincidence time with the tagger paddle which was hit (out of time showers must be dropped and the total energy recalculated); (3) no significant missing energy based on the photon energy for this tagger paddle (the elasticity cut); (4) the invariant mass reconstructed from the decay photons in the principle shower must be consistent with the  $\eta$ .

In this proposal, we only utilize exclusively produced  $\eta$ 's via the two-body  $\gamma p \rightarrow \eta p$  reaction. Once an  $\eta$  has passed our elasticity cut, the detection of the recoil proton is in principle redundant. However, we strongly suspect it would increase our sensitivity to be able to over-determine the kinematics. While a small amount of continuum  $\gamma p \rightarrow 2\pi^0 p$  will obviously pass the basic cuts, so could an accidental coincidence between a tagged  $\eta \rightarrow 2\gamma$  decay and  $\pi^0$  production by an untagged low energy photon. Either of these backgrounds would be suppressed by additional cuts using proton information: (5) there must be a single recoil proton, and (6) the recoil proton and  $\eta$  must be co-planar.

We are fortunate to have the GluEx detector to have the option of measuring recoil protons. As one can see from the top two panels of Figure 31, the recoil protons of interest have polar angles of 55-80 degrees and momenta of 0.2-1.4 GeV/c. Not all features of the reconstruction efficiency are currently understood; certainly the tracking algorithms were not optimized for low energy protons. Not surprisingly, there is little or no reconstruction efficiency below 0.275 GeV/c (40 MeV) where the range of a proton is only about 1.4 cm  $CH_2$ -equivalent. The  $LH_2$ , target walls, and start counter probably account for this. From Figure 32, one sees the tracking efficiency is a usable 60% near 0.3 GeV/c (48 MeV), increasing to a plateau of 80% for protons above 125 MeV of kinetic energy.

Because recoil protons are ejected at similar, large angles for all neutral meson masses, there is a tremendous amount of error magnification in reconstructing the missing mass from proton information. Nevertheless, we tried this and were pleasantly surprised to get the result in Figure 33 with missing mass resolution of about 100 MeV which is sufficient to usually distinguish between  $\pi^0$  and  $\eta$  production. These studies are in their infancy.

Once an  $\eta$  decay has been identified, they will be sorted into categories:  $\eta \rightarrow 2\gamma$  (normalization),  $\eta \rightarrow "3\gamma"$ , or  $\eta \rightarrow "4\gamma"$ . Although our  $\eta \rightarrow "4\gamma"$  dataset will be dominated by  $\pi^0 2\gamma$  plus a modest background, our physics goals require that we search for 3 signals:  $\pi^0 2\gamma$ ,  $2\pi^0$ , and  $4\gamma$  (only one  $\pi^0$ , two  $\pi^0$ 's, and no  $\pi^0$ 's). Since all 6 combinations of 2 photons must be tried, there are 6 opportunities for uncorrelated photons to mimic a  $\pi^0$ , thus the excellent resolution in  $\pi^0$  invariant mass demonstrated in the previous section is important for high sensitivity.

## 6 Infrastructure requirements

stand with vertical and horizontal motion capability for snake scans, cabling, Flash ADCs, power supplies,

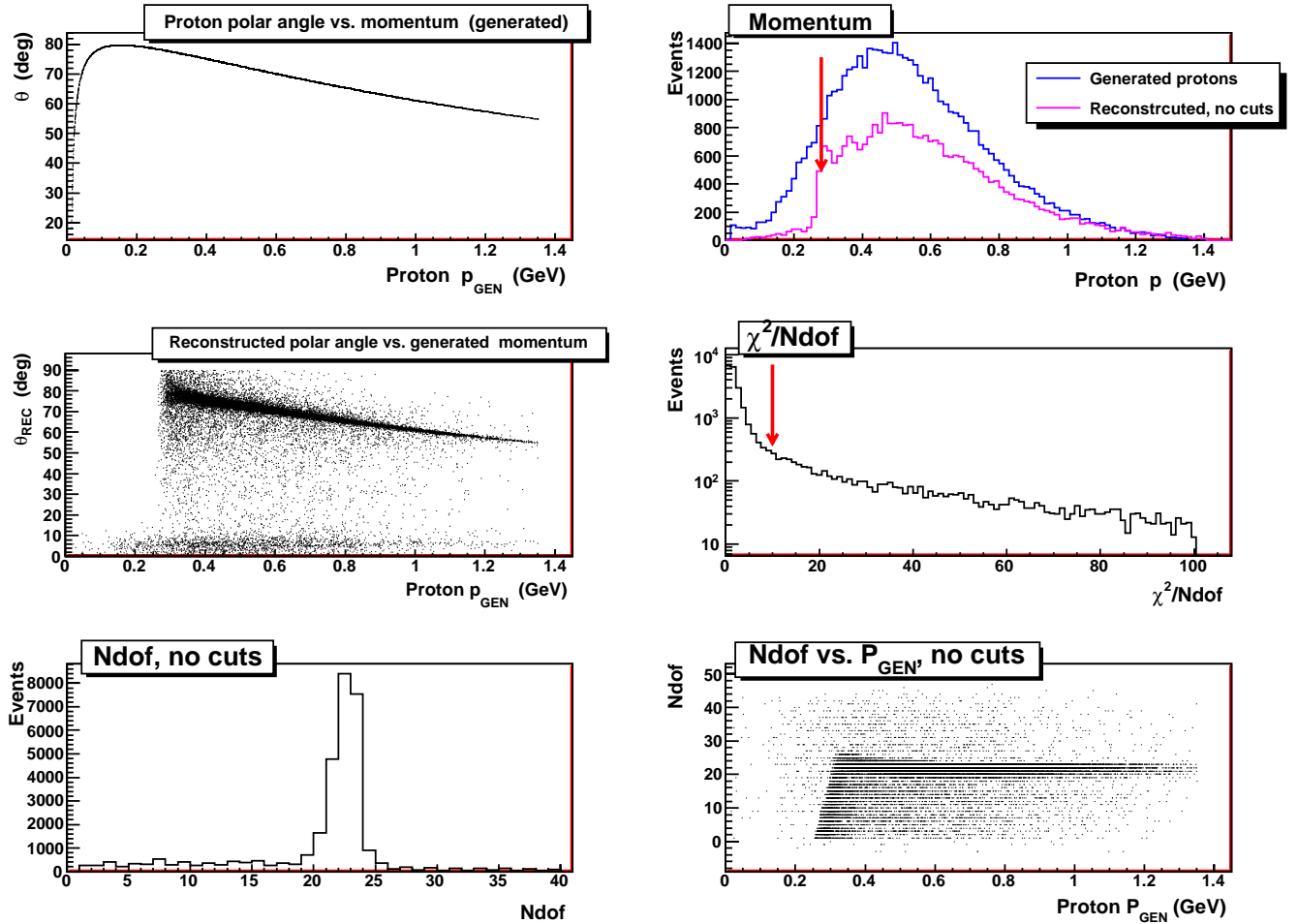


Figure 31: Monte Carlo simulation for detection of recoil protons by GluEx detector. Proton momenta are in units of GeV/c. Top-left panel: polar angle vs proton momentum; Top-right panel: momentum distribution of recoil protons (blue curve shows all events generated, red curve shows events reconstructed); Middle-left panel: reconstructed polar angle vs proton momentum; Middle-right panel: chi-squared per number of degrees of freedom (Ndof) distribution; Bottom-left panel: the Ndof distribution; Bottom-right panel: the Ndof vs. proton momentum.

## 7 $\eta$ Production Rate, Sensitivity, and Beam Request

The sensitivity of the experiment depends on the number of  $\eta$ 's which are exclusively produced (and hence which will survive the elasticity cut), the fraction of decays which are accepted by the calorimeter, and the efficiency including the live time and losses due to cuts.

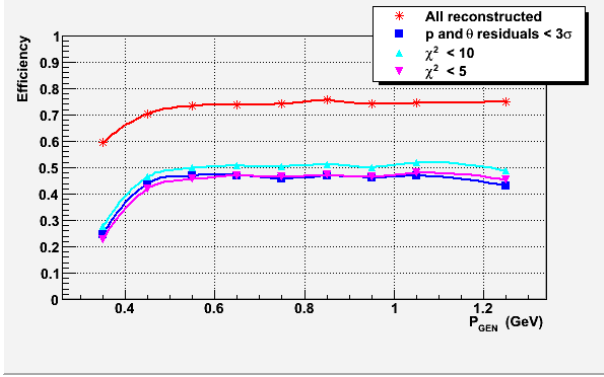


Figure 32: The reconstruction efficiency for recoil protons.

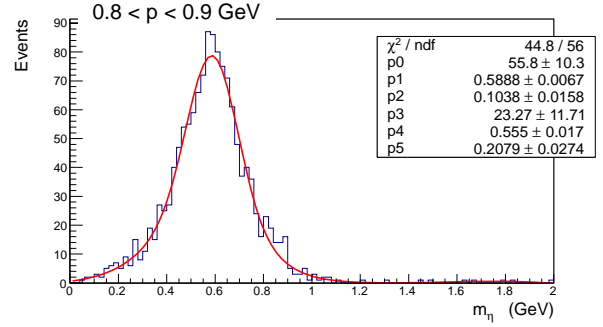


Figure 33: Reconstructed missing mass using the recoil proton from the  $\gamma p \rightarrow \eta p$  reaction.

## 7.1 $\eta$ production rate by forward $\gamma + p \rightarrow \eta + p$

We have chosen an electron beam current of  $0.4 \mu\text{A}$  with a Au radiator of thickness  $2 \times 10^{-4}$  to provide a luminosity comparable to the successful PrimEx program in Hall B.<sup>9</sup> Under these conditions, the so-called equivalent  $\gamma$  rate over a wide range of energy is  $\sim 5.0 \times 10^8$  Hz, or  $\sim 50$  MHz/GeV, three times less than the tagger design limit of 150 MHz/GeV. All photons are transported in vacuum. Using a 5 mm diameter primary collimator,  $\sim 30\%$  of the  $\gamma$ 's will reach the physics target, yielding a total  $\gamma$  rate at that location of  $1.5 \times 10^8$  Hz. In the 9.0–11.7 GeV photon energy range required for significant  $\eta$  cross sections and boost, the tagger focal plane provides 100% efficiency for tagging these photons in 30 MeV wide energy bins [30]. The tagged  $\gamma$  rate on the target will therefore be:

$$\begin{aligned} N_\gamma &= 1.5 \times 10^8 \times \ln(11.7\text{GeV}/9.0\text{GeV}) \\ &\sim 4 \times 10^7 \text{ Hz} \end{aligned}$$

We will use the standard Hall D LH<sub>2</sub> target. It is 30 cm thick (3.46% R.L.), hence the number of proton's in the target is:

$$N_p = 1.28 \times 10^{24} \text{ protons/cm}^2$$

From reference [44], the average total cross section for  $\gamma p \rightarrow \eta p$  in the 9 to 11.7 GeV photon energy range is  $\sim 70$  nb. The total rate of exclusively produced  $\eta$ 's by the golden channel  $\gamma + p \rightarrow \eta + p$  is therefore:

<sup>9</sup>The Hall D dump can handle up to  $2.2 \mu\text{A}$ .

$$\begin{aligned}
N_\eta &= N_\gamma \cdot N_p \cdot \sigma \\
&= 4 \times 10^7 \cdot 1.28 \times 10^{24} \cdot 70 \times 10^{-33} \\
&\sim 3.6 \text{ Hz (or } 3.1 \times 10^5 / \textit{day} \text{ or } 3.1 \times 10^7 / 100 \textit{ days} \text{ )}
\end{aligned}$$

Anticipating the detector acceptance results from the next section, the number of *effective*  $\eta$ 's ( $N_\eta \times \textit{Acceptance}$ ) will still be  $O(10^7)$  per year of JLab accelerator operations, several times the effective production rate of KLOE in its prime (using  $\phi \rightarrow \eta + \gamma$ ), and an order of magnitude better than BES-III (using  $J/\psi \rightarrow \eta + \gamma$ ).[45] This is the basis for our calling Hall D with FCAL-II an “ $\eta$  factory”.

## 7.2 detection rate of fully contained $\eta$ decays

Our reference design assumes that the transverse dimension of FCAL-II are  $118 \times 118 \text{ cm}^2$  and that it is located at 6 m downstream of the target center. The detected rate of an  $\eta$  decay depends on the number of  $\gamma$ 's in the final state. We will use copious  $\eta \rightarrow \gamma\gamma$  decays to normalize all other rare  $\eta$  decay channels (BR =  $39.43 \pm 0.26\%$  [8]). The acceptance for this channel is  $\sim 45\%$  thus the  $\eta \rightarrow \gamma\gamma$  detection rate will be:

$$\begin{aligned}
N_{\eta \rightarrow \gamma\gamma} &= 3.1 \times 10^5 / \textit{day} \times 0.3943 \times 0.45 \\
&\sim 5.5 \times 10^4 / \textit{day}
\end{aligned}$$

providing a statistical error on the normalization of less than 1% per day.

The rare decay  $\eta \rightarrow \pi^0\gamma\gamma$  has a branching ratio of  $2.7 \times 10^{-4}$  [8], bearing in mind that this is the average of several widely inconsistent measurements. Assuming the  $4\gamma$  final state follows phase space, the experimental acceptance is  $\sim 20\%$  hence the actual detection rate for  $\eta \rightarrow \pi^0\gamma\gamma$  will be:

$$\begin{aligned}
N_{\eta \rightarrow \pi^0\gamma\gamma} &= 3.1 \times 10^5 / \textit{day} \times 2.7 \times 10^{-4} \times 0.20 \\
&\sim 16.7 / \textit{day} \text{ or } 1670 / 100 \textit{ days}
\end{aligned}$$

Assuming the signal/background is 10:1 as suggested by simulations, the 1670 counts in 100 days would provide 10 bins in  $d\Gamma/dM_{\gamma\gamma}$  each with better than 10% statistical uncertainty. The final error on the  $\eta \rightarrow \pi^0 2\gamma$  branching ratio, including statistical and normalization errors, would be less than 5%.

EDITOR'S NOTE: NEED DGAMMA/DM2GAMMA PLOT BY OSET WITH OVERLAIN ERRORS (GAN)

If the P and CP forbidden  $\eta \rightarrow \pi^0\pi^0$  occurs according to phase space, the acceptance would be  $\sim 20\%$ . Table 3 contains nominal signal rates under various branching ratio assumptions. We assume the rare decay  $\pi^0 2\gamma$  is efficiently removed as a background by

demanding that two pairs of photons each reconstruct to the  $\pi^0$  mass. We saw earlier that the remaining background is dominated by the  $2\pi^0$  continuum, thus there will be approximately  $1670 \text{ events}/3 = 560$  candidate events since the S/B ratio was 3:1. Recoil proton cuts may further suppress the  $2\pi^0$  continuum but lacking those studies we'll proceed to estimate a BR upper limit sensitivity. Using signal and background estimates in the in the  $\eta$  invariant mass window:

$$BR \leq 2 \times \frac{\sqrt{N_{bkg}}}{N_\eta * Acceptance} = 2 \times \frac{\sqrt{560}}{3.1 \times 10^7 \times 0.2} = 8 \times 10^{-6} \quad (1)$$

This is about 1.5 orders of magnitude better than the existing upper limit for the neutral channel  $\eta \rightarrow 2\pi^0$ , and similar to what was achieved by KLOE for  $\eta \rightarrow \pi^+\pi^-$ .

Table 3: The nominal signal rate for the P and CP forbidden  $\eta \rightarrow \pi^0\pi^0$  with different branching ratio assumptions. The branching ratio in the first line is the present best upper limit[8].

Branching Ratio	Nominal Rate at BR (events/100 days)
$3.5 \times 10^{-4}$	2200
$10^{-5}$	62
$10^{-6}$	6

Similarly, Table 4 has been made for the C forbidden  $\eta \rightarrow \pi^0\gamma$  or  $3\gamma$  processes where the acceptance is a bit higher,  $\sim 30\%$ . We haven't studied these backgrounds as carefully as the  $4\gamma$  case. Simple arguments suggest that photon loss and merging backgrounds from  $\eta \rightarrow 3\pi^0$  are not the dominant backgrounds. More likely, the background will be due to a combination of photon splitting<sup>10</sup> from  $\eta \rightarrow 2\gamma \rightarrow 3\gamma$  or piled-up  $\eta \rightarrow 2\gamma$  events. These backgrounds are easily suppressed but the acceptance will be reduced. Assuming the background is 1/10 that of the previous case, but the effective number of  $\eta$ 's is reduced a factor of 2 by cuts, we have

$$BR \leq 2 \times \frac{\sqrt{N_{bkg}}}{N_\eta * Acceptance} = 2 \times \frac{\sqrt{56}}{3.1 \times 10^7/2 \times 0.3} = 3 \times 10^{-6} \quad (2)$$

This would be a factor of 5 better than the best result,  $1.6 \times 10^{-5}$ , but the estimate is only good to an order of magnitude.

---

<sup>10</sup>Photon splitting is where a shower is initiated by a single photon but reconstructs as a close pair. Obviously one can throw away all  $3\gamma$  candidates with close pairs, or where one of the photons is very low energy and/or near the beam hole hence more likely to be piled up.

EDITOR’S NOTE: UNTIL WE DO OUR HOMEWORK ON 3GAMMA, ALL WE CAN TRUTHFULLY SAY IS THAT WE’RE PROBABLY COMPETITIVE BUT WE JUST DON’T KNOW.

Table 4: The nominal signal rate for either C forbidden reaction leading to 3 photons in the final state for different assumptions about the branching ratio. The current BR upper limit for  $\eta \rightarrow 3\gamma$  is  $1.6 \times 10^{-4}$ , while that for  $\eta \rightarrow \pi^0\gamma$  is  $9 \times 10^{-5}$ [8].

Branching Ratio	Nominal Rate at BR (events/100 days)
$10^{-4}$	900
$10^{-5}$	90
$10^{-6}$	9

### 7.3 Beam Time Request

We request 100 days of beam time on the LH<sub>2</sub> target, plus commissioning and overhead as outlined below. This will provide about 1670 actual  $\eta \rightarrow \pi^0\gamma\gamma$  events, sufficient statistics to precisely measure the Dalitz plot of the  $2\gamma$  invariant mass. In the meantime, we’ll improve the upper limit on several SM forbidden channels by up to 2 orders of magnitude depending on the channel.

A summary of the requested beam time, specified for each major activity, is shown in Table 5. To understand backgrounds from the target windows and beamline sources such as the collimators (quasi-elastic protons, high energy neutrons, etc.) we need 7 days for both empty target and target-out runs. We will measure the tagging efficiency with the Total Absorption Counter and the pair-spectrometer several times. This will be interspersed

Table 5: Beam time request.

LH <sub>2</sub> production	100 days
Empty target and target-out runs	7 days
Tagger efficiency, TAC runs	3 days
FCAL-II commissioning, calibration, and checkout	12 days
Luminosity optimization (pile-up studies)	14 days
Total	136 days

with production and requires minimal configuration changes, hence only 3 days are budgeted. Based on our experience from the first PrimEx experiment in Hall B, we need 12 days for commissioning, calibration, and general checkout of FCAL-II with beam. The majority of this time will be used for the gain calibration and trigger setup including threshold adjustment. To be able to achieve the greatest possible sensitivity in 100 days of production, we further require 14 days to find the luminosity which optimizes our figure of merit  $N_\eta * Acceptance * Efficiency / \sqrt{N_{bkg}}$ .

## 8 The Collaboration and Contributions to Hall D

To be filled out when we get a list of institutions.

## 9 Summary

We expect to make revolutionary improvements to the dataset for  $\eta$  rare decays to all-neutral final states, addressing issues of chiral perturbation theory at high order while searching for new sources of C, P, and CP violation in non-weak decays of the best meson candidate for such studies. The availability of significantly boosted  $\eta$ 's in Hall D, and the planned lead tungstate calorimeter with flash ADC readout on every channel will improve the signal to background ratio by about 2 orders of magnitude. We estimate Hall D can produce  $3 \times 10^7$   $\eta$ 's in 100 days in the forward, exclusive channel  $\gamma + p \rightarrow \eta + p$  alone. Folding in the calorimeter acceptance of about 0.25, the effective number of  $\eta$ 's meets or exceeds that of other datasets of the last decade by a factor of several. However, the true figure of merit (FOM) must include backgrounds:  $N_\eta \times Acceptance / \sqrt{N_{bkg}}$ . This FOM for our conservative reference design will be up to 2 orders of magnitude *higher* than previous datasets mostly due to reduced backgrounds.

Non-conservatively, there is a possibility of an additional order of magnitude improvement in FOM by brute force. In that scenario, if we are able to double our acceptance by funding and building the larger 150cm x 150cm version of the calorimeter, and find during commissioning that we can run at a several times higher photon rate, then an additional 100 days of beam time would yield a dataset with 10x the FOM of the reference design in this proposal.

## 10 Opportunities for Theorists

EDITOR'S NOTE: THIS UNUSUAL SECTION MAY DISAPPEAR BY THE TIME THE PROPOSAL IS SUBMITTED. BUT WITH THIS DRAFT WE WANT OUR THEORY FRIENDS TO KNOW WHAT WE'RE THINKING

- The possible link between the ChPT parameters determined in  $\pi^0 2\gamma$  and the long distance correction in the rare kaon decays  $K \rightarrow \pi^0 l^+ l^-$  needs to be clarified.
- Bira Van Kolck is developing a generic expansion of T (thus CP) violating contributions to nuclear EDMs. His hope is to be able to understand what experiments constrain which terms, going beyond the lowest order - and apparently suppressed - contribution from the  $\theta_{QCD}$  term. A similar formalism for meson decays would be valuable. The contribution of the  $\theta_{QCD}$  term to  $\eta \rightarrow 2\pi^0$  is suppressed because it is proportional to  $(\theta_{QCD})^2$ . But how do the EDMs of quarks and gluons contribute in a generic SU(3) meson decay?
- It would be interesting to have a calculation of the allowed contribution of the 4-quark ( $s\bar{s}q\bar{q}$  where  $q$  is a lighter quark), CP violating operator to the decay  $\eta \rightarrow 2\pi^0$ .
- There are no calculations for the allowed decay  $\eta^0 \rightarrow 4\gamma$  which is a potential background in  $\pi^0 2\gamma$  measurement. By crude analogy with  $\pi^0 \rightarrow 4\gamma$  which has been rather thoroughly investigated by theorists, it appears  $\eta^0 \rightarrow 4\gamma$  is sufficiently suppressed that it will play no role, but one would like to put this on firmer ground.

## A Selection Rules for All-neutral $\eta$ Decays

The relevant masses and quantum numbers are given in Table 6. The results for different numbers of  $\gamma$ 's and  $p_i^0$ 's in the final state are summarized in Table 7. Because only neutral particles can be states of good C, any selection rules derived below assuming C conservation do not generally apply to  $\pi^\pm$ .

Table 6: Mass and quantum numbers for the  $\eta$ ,  $\pi^0$ , and  $\gamma$ .

Particle	Mass $(GeV/c)^2$	I	G	J	P	C
$\eta$	547.9	0	+1	0	-1	+1
$\pi^0$	135.0	1	-1	0	-1	+1
$\gamma$	0.0	0,1	-	1	-1	-1

### A.1 $\eta \rightarrow N\pi$

In this section we examine the selection rules for  $\eta \rightarrow N\pi$  and explain why  $\eta \rightarrow 3\pi$  is a major branch while the unobserved  $\eta \rightarrow 2\pi$  would be both P and CP violating.

Momentum and energy conservation allow  $\eta \rightarrow N\pi$  for  $N = 2, 3$ , and 4 only. Compared to the  $\eta \rightarrow 2\pi^0$  case which has similar selection rules, the decay  $\eta \rightarrow 4\pi^0$  is highly suppressed by phase space (the Q value would be only 7.9 MeV) and acceptance (with 8  $\gamma$ 's in the final state). Nefkens and Price [2] have nevertheless advocated the use of this channel due to relatively low backgrounds. While the  $4\pi^0$  case will be one of the ancillary rare decay channels searched for in this experiment, we will not discuss it in detail because our initial background simulations were done for 3 and 4 photon final states.

G-parity, approximately conserved only by the strong interaction, would require that  $G_\eta = G_{N\pi}$  or  $+1 = (-1)^N$  which is true only for even N.

Parity conservation, which in the Standard Model is generally assumed to be conserved by the strong and electromagnetic interactions and violated only by the weak interaction, would require that  $P_\eta = P_{N\pi} = P_\pi^N (-1)^L$  or  $-1 = (-1)^N (-1)^L$ . Because the  $\eta$  and  $\pi^0$  are spinless, conservation of total  $J = L + S = 0$  requires  $L = 0$  in the final state hence  $-1 = (-1)^N$ . Parity conservation therefore would allow  $\eta \rightarrow 3\pi$  (the only odd number of pions consistent with energy and momentum conservation) while the  $2\pi^0$  or  $4\pi^0$  final states would violate parity.

Table 7:  $\eta$  decays to  $\pi^0$ 's and  $\gamma$ 's. Branching ratios of observed states are given. Upper limits are quoted at 90% confidence level. Final states conserve C, P, and CP unless otherwise noted. The  $2\pi^0$  or  $4\pi^0$  final states would conserve C but violate P, CP. Final states with odd numbers of  $\gamma$ 's would violate C, however, for  $3\gamma$  both parity conserving and violating final states are possible.

	$0\pi^0$	$1\pi^0$	$2\pi^0$	$3\pi^0$	$4\pi^0$
$0\gamma$	–	–	PV, CPV $< 3.5 \cdot 10^{-4}$	allowed 32.6%	PV, CPV $< 6.9 \cdot 10^{-7}$
$1\gamma$	–	CV,CPV $< 9 \cdot 10^{-5}$	CV $< 5 \cdot 10^{-4}$	CV,CPV $< 6 \cdot 10^{-5}$	CV unknown
$2\gamma$	allowed 39.3%	allowed $2.7 \cdot 10^{-4}$	allowed $< 1.2 \cdot 10^{-3}$	allowed unknown	allowed unknown
$3\gamma$	CV $< 1.6 \cdot 10^{-5}$	CV unknown	CV unknown	CV unknown	CV unknown
$4\gamma$	allowed $< 2.8 \cdot 10^{-4}$	allowed unknown	allowed unknown	allowed unknown	allowed unknown

The conservation of C parity, usually assumed to hold for all but the weak interaction, would require  $C_\eta = C_{N\pi}$  or  $+1 = (+1)^N$  hence is conserved for all N.

Observations show [24] the  $\eta$  has a major decay branch to  $3\pi^0$  (33%). Clearly, conservation of G parity contributes to the long lifetime of the  $\eta$  by suppressing the strong interaction, but G parity is broken by isospin-violating strong interactions which conserve P. The  $2\pi^0$  branch, which would violate P conservation but conserve C and thus be CP violating, has never been observed with an upper limit of  $3.5 \cdot 10^{-4}$ . Because C conservation plays no role in  $\eta \rightarrow N\pi$  decays, the  $\pi^+\pi^-$  branch would also be P and CP violating and, presumably due to larger backgrounds for all-neutral decays in KLOE, has a more tightly constrained upper limit of  $1.5 \cdot 10^{-5}$ . Our goal is to achieve a branching ratio for  $\eta \rightarrow 2\pi^0$  of  $1 \cdot 10^{-6}$ , a reduction of 2 orders of magnitude for the  $2\pi^0$  branch or an improvement of 1 order of magnitude for *any*  $2\pi$  branch.

## A.2 $\eta \rightarrow M\gamma_{r,v}$

In this section we examine the selection rules for  $\eta \rightarrow M\gamma$  and explain why  $\eta \rightarrow 2\gamma$  is a major decay branch while  $\eta \rightarrow 3\gamma$  would violate C (while leaving the conservation of CP ambiguous). The same selection rules can be applied to reactions with final state pairs of  $e^+e^-$  or  $\mu^+\mu^-$  provided they arise from the usual suspect,  $\gamma_v \rightarrow l^+l^-$  (Dalitz decay).

Momentum and energy conservation allow  $\eta \rightarrow M\gamma$  for all M greater than 1.

C parity requires that  $C_\eta = C_{M\gamma}$  hence  $+1 = (-1)^M$ . Therefore, only even numbers of photons are allowed if C parity is conserved. Any odd number of photons implies a violation of C. This is an important and general rule which (anticipating the next section) holds for an arbitrary number of  $\pi^0$ 's in the final state because  $C_{\pi^0} = +1$ .

Briefly put, parity conservation effectively yields no constraints on the final number of photons. The rest of this paragraph contains the long version which you are welcome to skip: Parity conservation would require that  $P_\eta = P_{M\gamma} = P_\gamma^M (-1)^L$  or  $-1 = (-1)^M (-1)^L$ . Taking as an example the two-photon final state: parity conservation for this case gives  $-1 = (-1)^2 (-1)^L = (-1)^L$ . But what is L? Conservation of total angular momentum means  $J_f = L + S$  has to be coupled to 0 in the final state. Since two spin one photons can be coupled to  $S = 0, 1, \text{ or } 2$ , total  $J_f = 0$  requires  $L = 0, 1, \text{ or } 2$ , respectively. Because both even and odd values of L are available to the decay, a parity conserving reaction will select  $L = 1$  while a parity violating interaction will select  $L = 0$  or  $2$ . The status of the conservation of parity would therefore be ambiguous. (A corollary is that a parity-conserving decay option always exists, but if a new source of C violation were observed, it could be CP conserving or violating.) Similar arguments can be made for the case of more than two photons.

Observations show [24] that the  $\eta$  has a large branch to C-conserving  $2\gamma$  (39%). The smaller branching ratios to  $\gamma + e^+e^-$  ( $7 \cdot 10^{-3}$ ) and  $\gamma + \mu^+\mu^-$  ( $3.1 \cdot 10^{-4}$ ) can be quantitatively understood as the basic  $2\gamma$  process times  $\alpha$  and phase space factors. The fact that the  $2\gamma$  and  $3\pi^0$  branching ratios are comparable highlights the extent to which the strong interaction is suppressed in  $\eta$  decays. This suppression allows rare  $\eta$  decays to probe new sources of C, P, and CP violation above the (effectively zero) Standard Model floor. The C-violating  $3\gamma$  branch, which is a priority channel for us, has never been observed and has an upper limit of  $1.6 \cdot 10^{-5}$ .

A comment about the C-allowed  $4\gamma$  branch: it has never been seen with an upper limit of  $2.8 \cdot 10^{-4}$  hence it does not pose a significant potential background for our precision  $\pi^0 2\gamma$  measurement which has a branching ratio of  $2.7 \pm 0.5 \cdot 10^{-4}$  (the PDG result combines several experiments). A significantly improved measurement of the  $4\gamma$  branch will be another ancillary product of our program.

### A.3 $\eta \rightarrow N\pi^0 + M\gamma$

This section will only discuss cases *not* covered in the previous two sections (N,M each  $\geq 1$ ). None of these branches is large, but some of them are important for tests of chiral perturbation theory at high order or have potential for tests of C conservation.

Momentum and energy conservation are satisfied for  $N = 1,2,3,4$  and  $M = 1,2,\dots$ .

C parity conservation means  $C_\eta = C_{N\pi}C_{M\gamma}$  or  $+1 = (+1)^N(-1)^M = (-1)^M$ . There are no restrictions on the number of pions N but C is conserved for even numbers of photons and violated for odd numbers of photons.

Parity conservation can be written  $P_\eta = P_{N\pi}P_{M\gamma}(-1)^L$ , or  $-1 = (-1)^{N+M+L}$ . Two cases need to be discussed:

i. Single  $\gamma$  - Conservation of total angular momentum J requires the spin of the photon S and angular momentum L to couple to 0. The only possible value of L is 1 so  $-1 = (-1)^{N+1+1} = (-1)^N$ . Parity is therefore conserved for odd numbers of pions and violated for even numbers of pions. Although all single  $\gamma$  states would violate C, the CP state would alternate with the number of pions: the  $\pi^0\gamma$  state would violate CP, the  $2\pi^0\gamma$  state would conserve CP, and so on. The status of CP is only unambiguous in this one photon case.

ii. Two or more  $\gamma$ 's - As we saw in the section on  $\eta \rightarrow M\gamma$ , if there is more than one photon in the final state then the reaction can always select a value of L which conserves parity, or a different value of L which violate parity. The existence of the final state is not constrained by a parity selection rule. If the C violating  $3\gamma$  final state were observed, for

example, the status of P conservation and therefore CP would be ambiguous without a study of the angular correlation to determine L.

What is observed? The only observed channel in this class is  $\pi^0 2\gamma$  with branching ratio of  $2.7 \pm 0.5 \cdot 10^{-4}$ . This channel is a priority for us not only because it tests chiral perturbation theory at  $O(p^6)$  but because it is a “gateway” channel important for understanding the SM backgrounds in new physics searches such as  $\eta \rightarrow \pi^0 e^+ e^-$  and  $K_L^0 \rightarrow \pi^0 l^+ l^-$ .

Another allowed channel is  $2\pi^0 2\gamma$  which has a crude upper limit of  $1.2 \cdot 10^{-3}$ . This will be an ancillary rare decay channel in our experiment but the  $6\gamma$  final state has large backgrounds due to the copious branch  $\eta \rightarrow 3\pi^0$ .

There are several channels, for which only upper limits exist, with odd numbers of photons which would violate C. The simplest,  $\pi^0 \gamma$ , is absolutely forbidden by angular momentum selection rules and may therefore serve as an analysis control during the search for C violation in  $\eta \rightarrow 3\gamma$ . Ancillary channels searching for C violation include two yielding 5 photons in the final state ( $2\pi^0 \gamma$  and  $\pi^0 3\gamma$ ) and two yielding 7 photons ( $3\pi^0 \gamma$  and  $2\pi^0 3\gamma$ ). The 7 photon final states seem most promising since backgrounds from  $\eta \rightarrow 3\pi^0$  followed by photon splitting can be efficiently suppressed by cutting events with close showers in the calorimeter.

## References

- [1] M. Gell-Mann, R. J. Oakes, and B. Renner. Phys. Rev. 175 (1968) 2195.
- [2] B.M.K. Nefkens and J.W. Price, Phys. Scr. **T99** (2002) 114. This review ties is especially valuable for tying BR upper limits to model-independent constraints on C and CP violation in the strong and EM amplitudes.
- [3] S. Kullander *et al.*, Acta Physica Polonica B, Vol. 29 (1998) 97-111. This is an easy reading and insightful survey of the new physics potential of a broad, rare  $\eta$  decay program.
- [4] M. Unverzagt, Nucl. Phys. B (Proc. Suppl.) 198 (010) 174-181.
- [5] A. Kupsc *et al.*, Nucl. Phys. B (Proc. Suppl.) 181-182 (2008) 221-225.
- [6] M. Blanke, New Physics Sensitivity of Kaon Decays, Workshop on Fundamental Physics at the Intensity Frontier, Rockville, MD, Dec 2011.
- [7] F. Mescia, C. Smith, and S. Trine, JHEP **08** (2006) 088.
- [8] C. Amsler et al.(Particle Data Group), Phys. Lett., B667, 1 (2008).
- [9] M.N. Achasov et al., Nucl. Phys. B600, 3 (2001).
- [10] L. Ametller, J. Bijmens, A. Bramon and F. Cornet, Phys. Lett. B276, 185 (1992).
- [11] E. Oset, J.R. Pelaez, L. Roca, Phys. Rev. D77, 073001 (2008).
- [12] D. Alde et al., Yad. Fiz 40, 1447 (1984); D. Alde et al., Z. phys. C25, 225 (1984); L. G. Landsberg, phys. Rep., 128, 301 (1985).
- [13] S. Prakhov et al., Phys. Rev. C72, 025201(2005).
- [14] S. Prakhov et al., Phys. Rev. C78, 015206 (2008).
- [15] S. Prakhov, Proceeding of the 11th International Conference on Meson-Nucleon Physics and the Structure of the Nucleon, Juelich, 2007, <http://www.fz-juelich.de/ikp/menu2007/Program/ProgramSessions.shtml>.
- [16] B.Di Micco et al., Acta Phys. Slovaca 56, 403 (2006).
- [17] T.D. Lee and C.N. Yang, Phys, Rev. 104, 254 (1956); Z.K. Silagadze, Phys. At. Nucl. 60, 272 (1997).
- [18] C. Jarlskog and E. Shabalin, Phys. Rev. D52, 248 (1995)

- [19] C. Jarlskog and E. Shabalin, Phys. Rev. D52, 6327 (1995).
- [20] Particle Data Group, Phys. Rev., D66, (2002).
- [21] C. Jarlskog and E. Shabalin, Physica Scripta T99, 23 (2002).
- [22] C.Q. Geng *et al.*, Modern Physics Letters A, Vol. 17, No. 23 (2002) 1489-1497; and Dao-Neng Gao, Modern Physics Letters A, Vol.17 No. 24 (2002) 1583-1588.
- [23] E.L. Bratkovskaya *et al.*, Phys. Lett. B 359 (1995) 217-222.
- [24] K. Nakamura et al. (Particle Data Group), JPG **37**, 075021 (2010) and partial 2011 update for the 2011 edition.
- [25] K. Nakamura et al. (Particle Data Group), JPG **37**, 075021 (2010) and partial 2011 update for the 2011 edition. <http://pdg.lbl.gov/2011/tables/rpp2011-conservation-laws.pdf>
- [26] D.A. Dicus, Phys. Rev. D 12 (1975) 2133-2136.
- [27] J. McDonough et al, Phys. Rev. D 38 (1988) 2121.
- [28] A. Aloisio et al., Physics Letters B 591 (2004) 49-54.
- [29] B.M.K. Nefkens et al, Phys. Rev. C **72**, 035212 (2005).
- [30] The Technical Design of the Hall-D Polarized Photon Beam at the Thomas Jefferson National Accelerator Facility, The GlueX Collaboration, November 7, 2008.
- [31] Jefferson Lab Hall D CDR, version 5.0.
- [32] Silvia Niccolai, *Three-body photodisintegration of  $^3\text{He}$  measured with CLAS*, Ph.D. thesis, George Washington University, 2003, unpublished.
- [33] R. Bradford and R.A. Schumacher, CLAS-NOTE 2002-003, unpublished.
- [34] R.A. Schumacher, CLAS-NOTE 99-010, unpublished.
- [35] Mapping the Spectrum of Light Quark Mesons and Gluonic Excitations with Linearly Polarized Photons, The GlueX Collaboration, [gluex.org](http://gluex.org), July 2006.
- [36] Overview of Hall D solenoid refurbishment and testing, G. Biallas et al., September 2010.
- [37] Start Counter Update, W. U. Boeglin et al., Florida International University, February 2008.

- [38] The GLUEX Central Drift Chamber: Design and Performance, Y. Van Haarlem et al., NIM A, 622 (2010) 142–156.
- [39] Performance of the prototype module of the GlueX electromagnetic barrel calorimeter, B. D. Leverington et al., NIM A, 596 (2008) 327–337.
- [40] Time of Flight Detector, Conceptual Design Report, The GlueX Collaboration, March 2008.
- [41] J.V. Bennett, M. Kornicer, and M.R. Shepherd, Precision timing measurement of phototube pulses using a flash analog-to-digital converter, NIM A622, 225 (2010).
- [42] I. Larin et al., Phys. Rev. Lett., 106, 162303 (2011).
- [43] K. Nakamura et al. (Particle Data Group), J. Phys. G 37, 075021 (2010).
- [44] J.M. Laget, Phys Rev. **C72**, 022202 (2005).
- [45] M. Ablikim *et al.*, PRD **84**, 032006 (2011)
- [46] H. Beck et al., Nucl. Instr. Meth., A269, 568 (1988).
- [47] Jlab proposal “A Precision Measurement of the  $\eta$  Radiative Decay Width” (E-10-011), 2010.
- [48] A Measurement of Rare Radiative Decays of the  $\phi$  Meson, JLab Experiment E-94-016.
- [49] R.T. Jones *et al.*, Performance of the RADPHI detector and trigger in a high rated tagged photon beam, NIM A570 (2007) 384-398.
- [50] *ibid*, Compare Figures 1 and 2.